Quasi-static cyclic out-of-plane tests on masonry components 2016/2017

Damiola, Marina; Esposito, Rita; Ravenshorst, Geert

Publication date
2017

Document Version
Final published version

Citation (APA)
Damiola, M., Esposito, R., & Ravenshorst, G. (2017). *Quasi-static cyclic out-of-plane tests on masonry components 2016/2017*. Delft University of Technology.

Project number	C31B67
File reference	C31B67WP3-5
Date	5 December 2017
Corresponding author	Rita Esposito (r.esposito@tudelft.nl)

TU Delft Large-scale testing campaign 2016

QUASI-STATIC CYCLIC OUT-OF-PLANE TESTS ON MASONRY COMPONENTS 2016/2017

Authors: Marina Damiola, Rita Esposito, Geert J.P. Ravenshorst
Collaborators: Leonardo Bucci

***Cite as**: Damiola, M., Esposito, R., and Ravenshorst, G.J.P. Quasi-static cyclic out-of-plane tests on masonry components 2016/2017. Report No. C31B67WP3-5, 5 December 2017. Delft University of Technology.*

This research work was funded by NAM Structural Upgrading stream.

Table of Contents

1 Introduction

Quasi-static cyclic tests on masonry components, such as walls, can capture the behaviour of vulnerable elements and thus serve as benchmarks for the validation of analysis methods. They allow studying the response of the element in terms of load and deformation capacity, failure mechanism and hysteresis behaviour. In-plane and out-of-plane tests are generally performed in this category.

Considering their importance, these tests have been included in the large-scale testing campaign to be performed at Delft University of Technology in 2016 within the NAM Structural Upgrading project. The campaign includes a total of six work packages (WPs), which focus on the characterisation of vulnerable elements for both the detached and terraced house typology. In particular, for the detached house typology the behaviour of flexible diaphragms and theirs connection with solid clay brick masonry walls is investigated, while for the terraced house typology, the behaviour of buildings made of calcium silicate element masonry is investigated. These two topics are developed, respectively, in WP4 and WP5 with respect to the characterisation at connection, sub-assemblage and assemblage level. In WP3, which is here discussed, only the behaviour of URM masonry walls is studied; however choices related to geometry, materials and boundary conditions of the component tests are directly related to the other two WPs.

In this report the tests results related to the quasi-static cyclic out-of-plane tests on large-scale walls are presented. Quasi-static out-of-plane cyclic tests aim at studying the structural response of vulnerable members, which during an earthquake are placed perpendicular to the seismic action. The tests, performed in displacement control, allow determining the capacity curve of the member, in terms of lateral force and lateral displacement. The tests are designed to capture the two main out-of-plane failure mechanisms: one-way out-of-plane bending failure and two-way out-of-plane bending failure. The one-way out-of-plane bending failure can occurs in slender walls not laterally supported. The two-way out-of-plane bending failure usually generally occurs in squat walls supported on all four sides. This mechanism triggers a complex crack pattern, similar to a yield line envelop composed of horizontal and diagonal cracks, and thus results of importance for the validation of numerical models.

The report is composed of 9 sections. Section 2 lists the nomenclature adopted in this report. Section 3 reports a description of the out-of-plane tests performed in WP3. Section 4 gives an overview of the material properties determined via companion destructive tests. Section 5 presents the testing procedure for the out-plane tests on large-scale walls. Section 6 shows the experimental results in terms of hysteresis behaviour, force and displacement capacity and crack pattern. In Section 7, the initial stiffness of each wall is evaluated by adopting the analytical formulation; a comparison with experimental results and some consideration regarding the boundary conditions are presented. In Section 8, the maximum lateral capacity is estimated with analytical methods and compared with the experimental findings. Section 9 presents the assessment procedure currently proposed by the NEN-NPR 9998:2017 for the assessment of out-of-plane failure mechanism; its evaluation against the experimental findings is presented. Eventually, summary and conclusions are reported in Section 10.

2 Nomenclature

2.1 Symbols

α	Slope factor (as in Clause 7.4.4.2 of AS)
α_1 ; α_2	Bending moment coefficients taking into account the degree of fixity at the edges of the wall and the height-to-length ratio of the wall (as in Section 5.5.5 of EC6)
β	Crack height ratio coefficient
ΔF_f^i	Increment in lateral force given by friction between the wall and the airbags on the constant pressure side in each cyclic test
$\Delta F_{f,M27}$	Increment in lateral force given by friction between the wall and the airbags on the constant pressure side in the monotonic test
Φ	Capacity reduction factor (as in Clause 4.4 of AS),
η	Orthogonal ratio of the flexural strengths of masonry (as in Section 5.5.5 of EC6)
λ	Self-weight multiplier
ν	Poisson ratio of masonry in the direction perpendicular to bed joints
ξ_{SCC}	Seismic coefficient for the wall where the capacity equals seismic demands (as in Annex H of NEN-NPR)
σ_v	Overburden stress applied at the top of the wall during the out-of-plane test
a_f	Aspect factor (as in Clause 7.4.4.3, Table 7.5 of AS)
d	Mid-height displacement in each cyclic test
$d_{CR,M27}$	Critical mid-height displacement in the monotonic test on TUD_COMP-27
f_b	Normalised compressive strength of masonry unit
f_{bt}	Flexural strength of masonry unit
f_d	Minimum design compressive stress on the bed joints (as in Clause 7.4.3.3 of AS)
f_m	Compressive strength of masonry mortar
f_{mt}	Flexural strength of masonry mortar
f'_{mt}	Characteristic flexural tensile strength (as in Clause 3.3.3 of AS)
f'_t	Equivalent characteristic torsional strength (as in Clause 7.4.4.3 of AS)
f'_{ut}	Characteristic lateral modulus of rupture of the masonry units (as in Clause 3.2 of AS)
f_{x1}	Masonry flexural strength with the moment vector parallel to the bed joints and in the plane of the wall, which generates a plane of failure parallel to the bed joints
f_{x2}	Masonry flexural strength with the moment vector orthogonal to the bed joints and in the plane of the wall, which generates a plane of failure perpendicular to the bed joints
g	Gravitational acceleration
h_u	Height of masonry unit
k_p	Perpend spacing factor (assessed in accordance with Clause 7.4.3.4 of AS)
k_1	Coefficient (as in Clause 7.4.4.3, Table 7.5 of AS)
k_2	Coefficient (as in Clause 7.4.4.3, Table 7.5 of AS)
l_u	Length of masonry unit
p^i	Pressure of the airbag on the North side in each cyclic test

$p_{M\,27}$	Pressure of the airbag on the North side in the monotonic test on TUD_COMP-27
r_b	Ratio between the bottom and mid-height horizontal displacement (recorded by the sensors S1, S4 and S2, S5 for one-way bending test and S6A and S5A for two way bending tests)
r_t	Ratio between the top and mid-height horizontal displacement (recorded by the sensors S3, S6 and S2, S5 for one-way bending test and S4A and S5A for two way bending tests)
t_u	Thickness of masonry unit
t_j	Thickness of mortar joint
t_w	Thickness of the wall
t_w^i	Thickness of the wall in each cyclic test
$t_{w,M\,27}$	Thickness of the wall in the monotonic test on TUD_COMP-27
u	Mid-height displacement of the wall
u_{cr}	Mid-height displacement at onset of cracking
w_{AS}	Lateral load capacity of the wall (as in Clause 7.4.4.2 of AS)
w_E	Maximum lateral load per unit area (as in Section 5.5.5 of EC6)
w_{cr}	Lateral pressure at onset of cracking
z	Height of gravity centre of the wall above top of the foundation (as in Annex H of NEN-NPR)
E_1	Secant elastic modulus of masonry subject to a compressive loading perpendicular to the bed joints, evaluated at 1/3 of the maximum stress
E_2	Secant elastic modulus of masonry subject to a compressive loading perpendicular to the bed joints, evaluated at 1/10 of the maximum stress
E_3	Chord elastic modulus of masonry subject to a compressive loading perpendicular to the bed joints, evaluated at between 1/10 and 1/3 of the maximum stress
F	Lateral force on the wall
F_{EC6}	Lateral force on the wall according to EC6
F_{AS}	Lateral force on the wall according to AS
F_{cr}	Lateral force at onset of cracking
G_c	Assumed slope of the crack line (as in Clause 7.4.4.2 of AS)
$H_{building}$	Height of the building above top of the foundation (as in Annex H of NEN-NPR)
H_d	Design height of the wall (as in Clause 7.4.4.2 of AS)
H_{eff}	Effective height of the wall
H_w	Height of the wall
I	Inertia moment of the wall (axis parallel to bed joints and in the plane of the wall)
K_{in}	Initial stiffness of the wall
L_d	Design length when both vertical edges are laterally supported (as in Clause 7.4.4.2 of AS)
L_w	Length of the wall
M_{ch}	Horizontal bending moment capacity of a wall (as in Clause 7.4.3.2 of AS)
M_{cd}	Diagonal bending moment capacity per unit length of diagonal crack (as in Clause 7.4.4.3 of AS)
$M_{E,1}$	Maximum moment of a masonry wall loaded in two-way bending when the plane of failure is parallel to the bed joints in the f_{x1} direction (as in Section 5.5.5 of EC6)
$M_{E,2}$	Maximum moment of a masonry wall loaded in two-way bending when the plane of failure is perpendicular to the bed joints in the f_{x2} direction (as in Section 5.5.5 of EC6)

N	Pre-compression force on the wall
R_{f1}	Restraint factor for the first supported edge of the wall (as in Clause 7.4.4.2 of AS)
R_{f2}	Restraint factor for the second supported edge of the wall (as in Clause 7.4.4.2 of AS)
$S_{a;d}$	Design seismic coefficient for the wall (as in Annex H of NEN-NPR)
T_a	Fundamental period of the wall (as in Annex H of NEN-NPR)
T_1	Fundamental period of the building (as in Annex H of NEN-NPR)
$S_{a;d} / \alpha$	Amplification factor (as in Annex H of NEN-NPR)
W	Self-weight of the wall
Z	Elastic section modulus of a unit height or length of the wall (as in Section 6.3 of EC6)
Z_d	Section modulus of the bedded area (as in Clause 7.4.3.2 of AS)
Z_p	Lateral section modulus based on the mortar contact area of the perpend joints (as in Clause 7.4.3.2 of AS)
Z_t	Equivalent torsional section modulus measured normal to the diagonal crack line (as in Clause 7.4.4.3 of AS)
Z_u	Lateral section modulus of masonry units (as in Clause 7.4.3.2 of AS)

2.2 Abbreviations

Avg.	Average
AS	Australian Standard
C.o.V.	Coefficient of variation
CS	Calcium silicate
EC6	Eurocode 6
NEN-NPR	Nederlands Normalisatie-instituut - Nederlandse-praktijkrichtlijnontwerp
OOP	Out-of-plane
St. dev.	Standard deviation

3 Description of the specimens

Four masonry walls, listed in Table 1, were tested under quasi-static out-of-plane cyclic tests. For the solid clay brick masonry, two specimens were tested: one single wythe wall (TUD_COMP-26) and one double-wythe wall (TUD_COMP-27). The two-way out-of-plane bending failure mechanism was investigated. Two walls made of calcium silicate element masonry were tested: one slender wall (TUD_COMP-28) to investigate the one-way out-of-plane failure and one squat wall (TUD_COMP-29) to study the two-way out-of-plane failure mechanism. Table 1 and Figure 1 show an overview of the tested walls.

Table 1 – Overview of quasi-static cyclic out-of-plane tests.

Sample name	Units type and size	L_w	H_w	t_w	Overburden	Boundary conditions
	mm	mm/units	mm/units	mm	MPa	
TUD_COMP-26	Solid clay brick 210x100x50	3950/18	2710/45	100	0.06	2-way OOP
TUD_COMP-27	Solid clay brick 210x100x50	3840/17.5	2710/45	210	0.06	2-way OOP
TUD_COMP-28	CS elements min548-max897x120x643	1448/2	2725/4	120	0.25	1-way OOP
TUD_COMP-29	CS elements min447-max897x120x643	3597/5	2725/4	120	0.06	2-way OOP

(a) (b) (c)

Figure 1 – Overview of quasi static cyclic out-of-plane tests: (a) TUD-COMP_26, (b) TUD-COMP_28 and (c) TUD-COMP_29.

4 Material properties

The characterisation of every masonry type has been carried out by performing destructive laboratory tests on both masonry and its constituents. The aim of these tests is twofold: 1) to serve as companion tests for the large-scale tests on components (WP3) and assemblage (WP5), 2) to study the correlation between various material testing methods (WP1).

In this study three masonry types have been studied: (1) calcium silicate element masonry, (2) single wythe solid clay brick masonry and (3) double wythe solid clay brick masonry.

In Table 2 and Table 3 the material properties of calcium silicate element masonry and solid clay brick are reported. Detailed information on the tests can be found in the dedicated reports [1] and [2].

Table 2 – Material properties of CS element masonry.

Property		Symbol	Unit	Average	St. dev.	C.o.V.
Compressive strength of mortar		f_m	MPa	**16.1**	1.48	0.09
Flexural strength of mortar		f_{mt}	MPa	**4.7**	1.04	0.22
Compressive strength of masonry unit		f_b	MPa	**19.4**	2.69	0.14
Flexural strength of masonry unit		f_{bt}	MPa	**3.65**	0.21	0.06
Elastic modulus of masonry unit in compression		E_b	MPa	**8916**	7624	0.11
Density of masonry		ρ	Kg/m^3	**1824**	38	0.02
Compressive strength of masonry in the direction perpendicular to bed joints		f'_m	MPa	**13.93**	1.03	0.07
Elastic modulus of masonry in the direction perpendicular to bed joints evaluated	at 1/3 of the maximum stress	E_1	MPa	**8557**	1619	0.19
	at 1/10 of the maximum stress	E_2	MPa	**9256**	2660	0.29
	between 1/10 and 1/3 of the maximum stress	E_3	MPa	**8313**	1251	0.15
Fracture energy in compression for loading perpendicular to bed joints		$G_{f\text{-}c}$	N/mm	**20.9**	5.47	0.26
Poisson ratio of masonry in the direction perpendicular to bed joints		ν	-	**0.21**	0.04	0.20
Strain corresponding to peak strength in compression in the direction perpendicular to bed joints		ε_p	‰	**2.01**	0.37	0.19
Compressive strength of masonry in the direction parallel to bed joints		$f'_{m,h}$	MPa	**9.42**	1.63	0.17
Elastic modulus of masonry in the direction parallel to bed joints		$E_{1,h}$	MPa	**8416**	1445	0.17
		$E_{2,h}$	MPa	**10524**	1625	0.15
		$E_{3,h}$	MPa	**7701**	1502	0.19
Fracture energy in compression for loading parallel to bed joints		$G_{f\text{-}c,h}$	N/mm	**12.8**	4.34	0.34
Strain corresponding to peak strength in compression in the direction parallel to bed joints		$\varepsilon_{p,h}$	‰	**1.58**	0.39	0.24
Masonry flexural strength with the moment vector parallel to the bed joints and in the plane of the wall		f_{x1}	MPa	**0.58**	0.08	0.14
Masonry flexural strength with the moment vector orthogonal to the bed joint and in the plane of the wall		f_{x2}	MPa	**0.73**	0.03	0.04
Masonry flexural strength with the moment vector orthogonal to the plane of the wall		f_{x3}	MPa	**0.41**	0.07	0.17
Flexural bond strength		f_w	MPa	**0.55**	0.09	0.17
Masonry (bed joint) initial shear strength		f_{v0}	MPa	**0.83**	-	-
Masonry (bed joint) shear friction coefficient		μ		**1.48**	-	-

Table 3 – Material properties of solid clay brick masonry.

Property		Symbol	Unit	Single wythe			Double wythe		
				Average	St. dev.	C.o.V.	Average	St. dev.	C.o.V.
Compressive strength of mortar		f_m	MPa	**3.81**	0.34	0.09	See single wythe		
Flexural strength of mortar		f_{mt}	MPa	**1.40**	0.17	0.12			
Compressive strength of masonry unit		f_b	MPa	**28.31**	2.92	0.10			
Flexural strength of masonry unit		f_{bt}	MPa	**6.31**	0.72	0.11			
Elastic modulus of masonry unit		E_b	MPa	**8049**	423	0.05			
Density of masonry		ρ	Kg/m^3	**1708**	71	0.04			
Compressive strength of masonry in the direction perpendicular to bed joints		f'_m	MPa	**14.02**	0.56	0.04	**9.24**	1.26	0.14
Elastic modulus of masonry in the direction perpendicular to bed joints evaluated	at 1/3 of the maximum stress	E_1	MPa	**4380**	605	0.14	**2771**	496	0.18
	at 1/10 of the maximum stress	E_2	MPa	**4068**	783	0.19	**2646**	970	0.37
	between 1/10 and 1/3 of the maximum stress	E_3	MPa	**4590**	603	0.13	**2951**	431	0.15
Fracture energy in compression for loading perpendicular to bed joints		$G_{f\text{-}c}$	N/mm	**28.52**	3.40	0.12	**34.8**	8.1	0.23
Poisson ratio of masonry in the direction perpendicular to bed joints		ν	-	**0.14**	0.02	0.11	**0.11**	0.02	0.21
Strain corresponding to peak strength in compression in the direction perpendicular to bed joints		ε_p	‰	**4.3**	0.40	0.10	**4.06**	0.70	0.19
Compressive strength of masonry in the direction parallel to bed joints		$f'_{m,h}$	MPa	**13.11**	2.41	0.18	**9.15**	0.91	0.10
Elastic modulus of masonry in the direction parallel to bed joints		$E_{1,h}$	MPa	**3332**	565	0.17	**4012**	676	0.17
		$E_{2,h}$	MPa	**3664**	689	0.19	**3954**	516	0.13
		$E_{3,h}$	MPa	**3207**	592	0.18	**4319**	1571	0.36
Fracture energy in compression for loading parallel to bed joints		$G_{f\text{-}c,h}$	N/mm	**35.1**	6.63	0.19	**28.3**	4.3	0.15
Strain corresponding to peak strength in compression in the direction parallel to bed joints		$\varepsilon_{p,h}$	‰	**5.8**	1.0	0.19	**4.6**	0.9	0.21
Masonry flexural strength with the moment vector parallel to the bed joints and in the plane of the wall		f_{x1}	MPa	**0.16**	0.03	0.21	**0.14**	0.05	0.31
Masonry flexural strength with the moment vector orthogonal to the bed joint and in the plane of the wall		f_{x2}	MPa	**0.65**	0.19	0.28	**0.41**	0.06	0.15
Masonry flexural strength with the moment vector orthogonal to the plane of the wall		f_{x3}	MPa	**0.46**	0.09	0.22	**0.42**	0.05	0.47
Flexural bond strength		f_w	MPa	**0.15**	0.05	0.32	See single wythe		
Masonry (bed joint) initial shear strength		f_{v0}	MPa	**0.20**	**-**	-			
Masonry (bed joint) shear friction coefficient		μ	-	**0.69**	**-**	-			
Residual masonry (bed joint) initial shear strength		$f_{v0,res}$	MPa	**0.05**	**-**	-			
Residual masonry (bed joint) shear friction coefficient		μ_{res}	-	**0.60**	**-**	-			

5 Testing protocol

In this Section the testing protocol is presented. The protocol is similar to the one adopted for the tests carried out in the large-scale testing campaign at Delft University of Technology in 2015 [3]. However, few modifications have been implemented with respect to the boundary conditions and the reaction frame. Section 5.1 reports the test set-up for both one-way and two-way out-of-plane bending tests, Section 5.2 reports the loading scheme and Section 5.2 describes the measurement system.

5.1 Test set-up

Figure 2 shows the out-of-plane test set-up for slender walls subject to one-way out-of-plane test. The wall is built within a steel frame composed by two beams with rectangular hollow section placed at the top and bottom of the wall and two lateral columns. The top beam is connected to the column via spring which will be used to apply the overburden. The wall within its steel frame is placed in the set-up by connecting the top and bottom steel beam to cross beams. At the bottom the cross beams are connected to the transversal beams, while at the top glass plates are installed between the cross beams and the transversal beams to allow the vertical translation of the wall. The cross section of the top and bottom beams was selected as a 300x300-mm rectangular tube profile, to be rotationally stiff.

Figure 3 shows the test set-up for squat walls subject to two-way out-of-plane bending test. Similarly to the slender wall, the squat wall is built within a steel frame. Additionally to the constraints imposed for the slender wall, the squat wall is laterally constrained with hinged connection (Figure 4). The lateral hinged connection is applied by adopting steel tubes of 100x80x4-mm at the edge of the wall on both the North and South side. The steel tubes are fixed at the bottom beam and connected to the external steel frame in two points. In order to prevent damage due to the interaction between the steel tubes and the masonry wall, wooden wedges are adopted.

Before the test an overburden was applied at the top of the walls by pre-tensioning the spring connecting the top steel beam and the lateral columns. The constant vertical load takes into account the weight of the top steel beam, the weight of the cross beams and the springs load. Four vertical springs, each of them having a stiffness of 50 kN/m, connect the top and bottom steel beams allowing vertical movements of the wall during out-of-plane deformations. In order to allow the vertical movement, glass plates with reduced friction are placed between the top cross beams and the transversal beam of the set-up (Figure 5). An overview of the imposed overburden is given in Table 4.

A uniform lateral load is applied using airbags on both north and south side of the wall. In the case of the one-way bending test, one airbag having dimension 1400x2600-mm is used. In the case of the two-way bending test, two airbags having dimension 1400x2600-mm are used on the lateral part of the wall, while two airbag having dimension 500x2600-mm are used in the central part of the wall (Figure 6). In both cases a timber reaction frame having dimensions 4000x2710-mm is adopted to measure the applied load. The timber reaction frame is designed to have a maximum deformation of 10 mm, which is much lower than the maximum deformation of the airbags (100 mm). The lateral forces were measured against the timber reaction frame with four load cells on both sides for wall TUD_COMP-26 and wall TUD_COMP-28 and with eight load cells on both sides for wall TUD_COMP-27 and wall TUD_COMP-29. During the test, due to the presence of the airbags and the timber reaction frame, the propagation of the cracks cannot be observed.

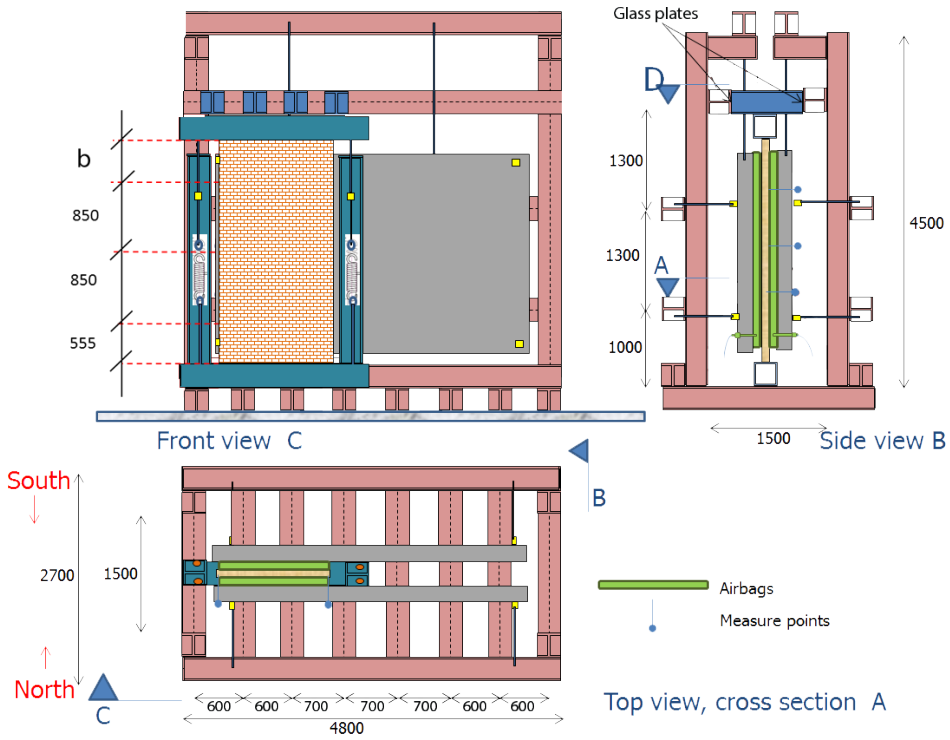

Figure 2 – Test set-up for slender walls subject to one-way out-of-plane cyclic test.

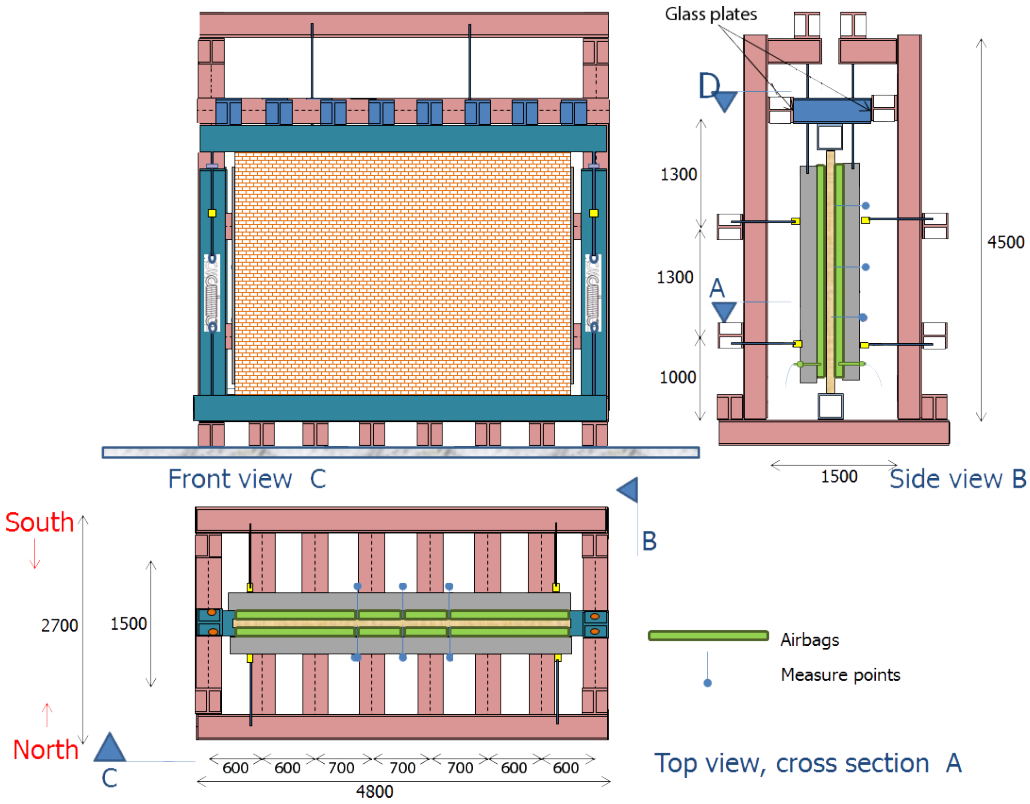

Figure 3 – Test set-up for squat walls subject to two-way out-of-plane cyclic tests.

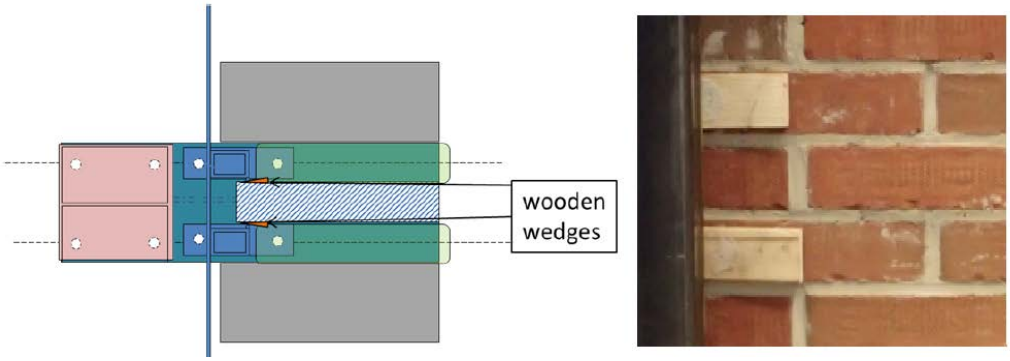

Figure 4 – Detail of lateral constraints for two-way out-of-plane bending test.

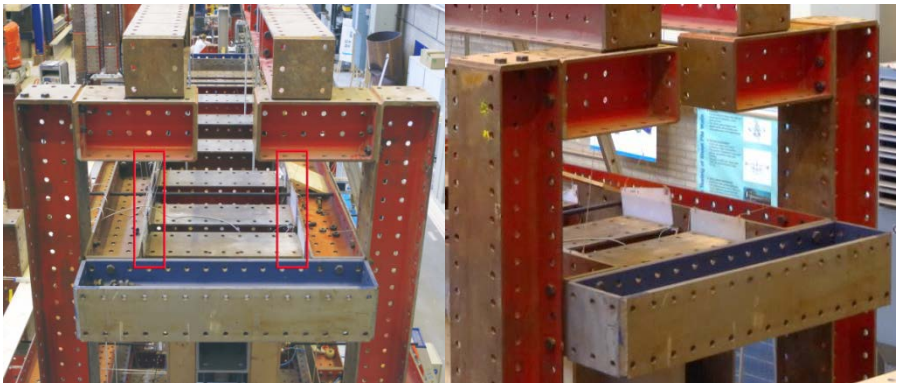

Figure 5 – Detail of glass plates placed between the top cross beams and the transversal beam.

Table 4 – Overview of the overburden in the quasi-static cyclic out-of-plane tests.

Sample name	Overburden	Weight top beam	Weight cross beams	Force for each spring
	MPa	kN	kN	kN
TUD_COMP-26	0.06 (23.70 kN)	8.0	7.93	1.94
TUD_COMP-27	0.06 (48.38 kN)	8.0	7.93	8.11
TUD_COMP-28	0.25 (43.44 kN)	4.0	3.97	8.87
TUD_COMP-29	0.06 (25.90 kN)	8.0	7.93	2.49

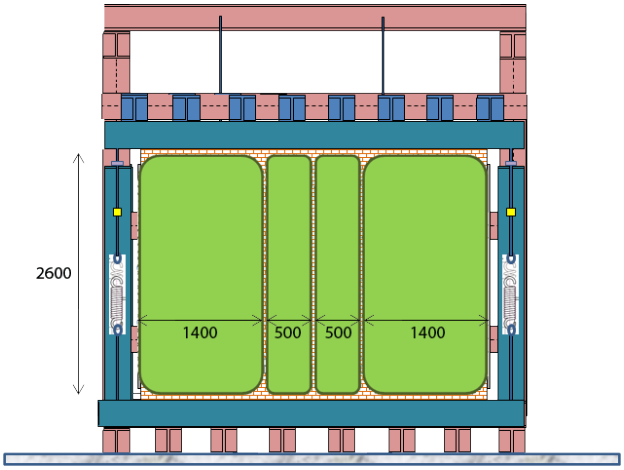

Figure 6 - Positioning of the airbags.

5.2 Instrumentation

Table 5 and Figure 7 show an overview of the main measurement points used for the out-of-plane tests. The measurement system has been designed to record:

- the applied vertical force on the wall through load cells FV1-FV4.
- the lateral force against the timber reaction frame at selected locations through load cells FN1-FN8 (north side) and FS1-FS8 (south side). The load cells are connected directly to the external steel frame through steel bars of 20 mm diameter.
- the out-of-plane horizontal displacements of the wall through linear potentiometers S1-S9. The displacements are recorded with respect to an independent reference system not in contact with the testing frame. The displacement and the reaction forces are measured with respect to two different independent reference systems. In some cases, sensors with a higher precision are adopted (denoted with letter A). The position of the measurement points is chosen in compatibility with the airbags dimensions. Holes are made in the timber reaction frame to allow the connection of the linear potentiometers to the wall.
- the pressure in the airbag system on North side (Press).
- the rotation of the bottom beam on which the masonry wall is glued. For this purpose linear potentiometers (Frame1N, Frame1S, Frame2N, Frame2S) are used to measure the vertical displacement at the two side of the bottom beam with respect to the cross beams. The measurement is made at two positions along the wall.
- the rotation of the top beam on which the masonry wall is glued. For this purpose linear potentiometers (TopV1N, TopV1Z, TopV2N and TopV2, Figure 8) are used to measure the vertical displacement at the two side of the top beam with respect to the cross beams. The measurement is made at two positions along the wall.
- the horizontal relative displacements between the top cross beams and the set-up frame. For this purpose linear potentiometers (TopH1N, TopH1S, TopH2N and TopH2S, Figure 8) are used at two locations. These sensors are used to measure the effectiveness of the top support in which the glass plate should allow vertical movement of the wall. The sensors have been adopted only for the two-way bending tests.
- the opening of the cracks. Sensors (CR1N-CR5N and CR1S-CR5S) are placed on the thickness of the wall. The sensors have been adopted only for the only for one-way bending test.

The applied lateral load is calculated as the difference between the total force measured on the south side and the one measured on the north side ($F = \Sigma FS - \Sigma FN$).
Table 3 summarizes the distances, called a and b in Figure 7, between sensors S1-S9.

Table 5 - Overview of the measurement system of the out-of-plane tests.

Name	Description	Sensor Type	Capacity (kN) or Stroke (mm)
FV1, FV3	Vertical force in springs on North side.	Load cell	10 kN
FV2, FV4	Vertical force in springs on South side.	Load cell	10 kN
FN1-FN8 and FS1-FS8	Horizontal forces on reaction frame on North side and South side.	Load cell	25 kN
S1-S9	Horizontal displacement of the wall.	Linear potentiometer	±110 mm
S5A and S2A (one-way) or S4A, S5A and S6A (two-way)	Horizontal displacement of the wall.	Linear potentiometer	±50 mm
TopV1N, TopV2N, TopV1S, TopV2S	Vertical displacement of the top beam.	Linear potentiometer	±19 mm
TopH1N, TopH2N, TopH1S, TopH2S	Horizontal displacement of the top beam.	Linear potentiometer	±19 mm
Frame1N, Frame1S, Frame 2N, Frame2S	Vertical displacement of the bottom beam.	Linear potentiometer	±19 mm
CR1N-CR5N and CR1S-CR5S (one-way)	Opening of the cracks on the North side and South side.	Linear potentiometer	±19 mm

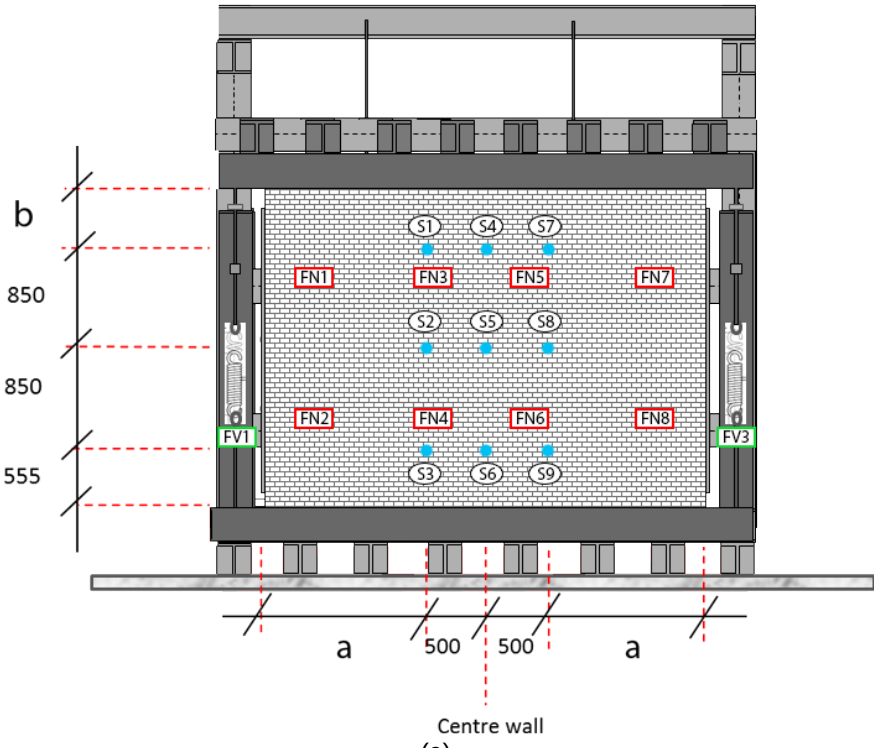

(a)

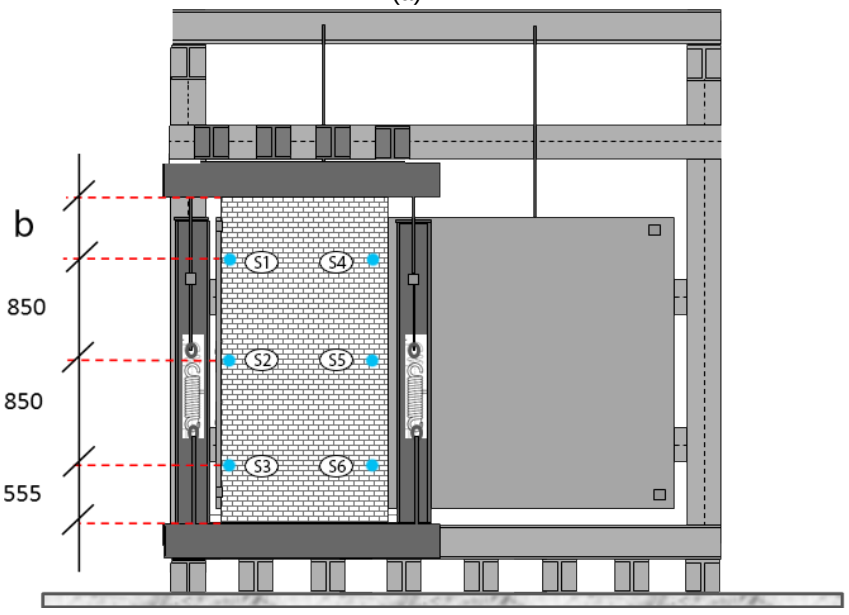

(b)

Figure 7 – Measurement system on the north side: (a) location of load cells and horizontal displacement sensors S1-S9 for two-way bending test, (b) location of horizontal displacement sensors S1-S6 for one-way bending test.

Table 6 – Distances between sensors S1-S9 (see Figure 7).

Specimen	a (mm)	b (mm)
TUD_COMP-26	1475	455
TUD_COMP-27	1420	455
TUD_COMP-28	-	505
TUD_COMP-29	1300	455

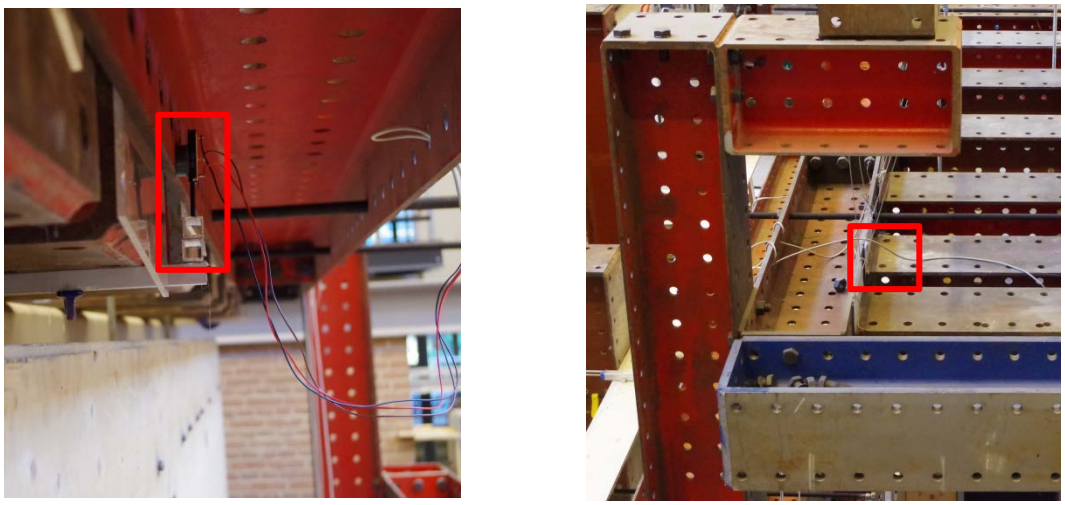

(a) (b)

Figure 8 – Displacement sensors of the top beam: (a) vertical TopV1N, TopV2N, TopV1S, TopV2S; (b) horizontal TopH1N, TopH2N, TopH1S, TopH2S.

5.3 Loading scheme

The test is performed in displacement control by controlling the mid-point displacement. In the case of the one-way bending test, the mid-point displacement is defined as the average of the two displacements measured at the mid-height of the wall on the left and the right side of the wall (sensors S2 and S5, see Section 5.2). In the case of the two-way bending test, the mid-point displacement is defined as the displacement of the central point (sensor S5, see Section 5.2). The displacement at the mid-point is cyclically varied. Every cycle is composed by three identical runs; in every run the horizontal displacement is varied in both directions starting and ending at the zero position, which is the initial position of the wall (Figure 9). In every run the displacement is first applied in the positive loading direction (from south to north) and afterwards in the negative loading direction (from north to south). Test set-up is capable to achieve a centre displacement of +/- 100 mm. If this can be reached in the test depends on the stability of the walls.

Figure 10 shows the loading scheme for the application of the uniform horizontal load in the case of squat walls; for the slender walls the same loading scheme is used. The airbags on the South and North side are pumped up to a certain initial pressure before stating the test. During the test the initial pressure is kept constant in the airbags on the North side, while the pressure increases in the airbags on the South side due to imposed displacement. The initial pressure is chosen in order to prevent negative pressure in the airbags placed at the South side. The load acting on the wall is determined as the difference between the load on the South and North side.

The net contact area between the wall and the airbag is calculated considering the total force measured by the load cells on the North side and the pressure measured in the airbags on the North side (A_{net} = ΣFN/Press). By considering as a reference the area of the airbag in their uninflated condition A_{airbag}, it was observed that the net contact area A_{net} during the test was approximatively 90 and 75-80% of the reference area in the case of the slender and squat wall, respectively. These results are in line with the values found in the previous experimental campaign [3] for which values of 86 and 76% were reported for the slender and squat walls, respectively. Similar values were also reported by Griffith et al. [4] for squat walls.

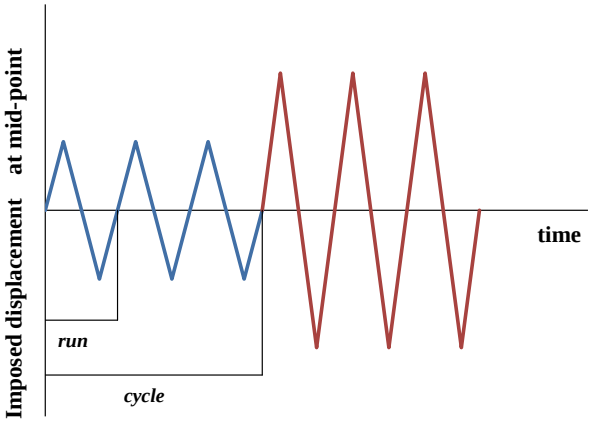

Figure 9 – Loading scheme: cycles and runs.

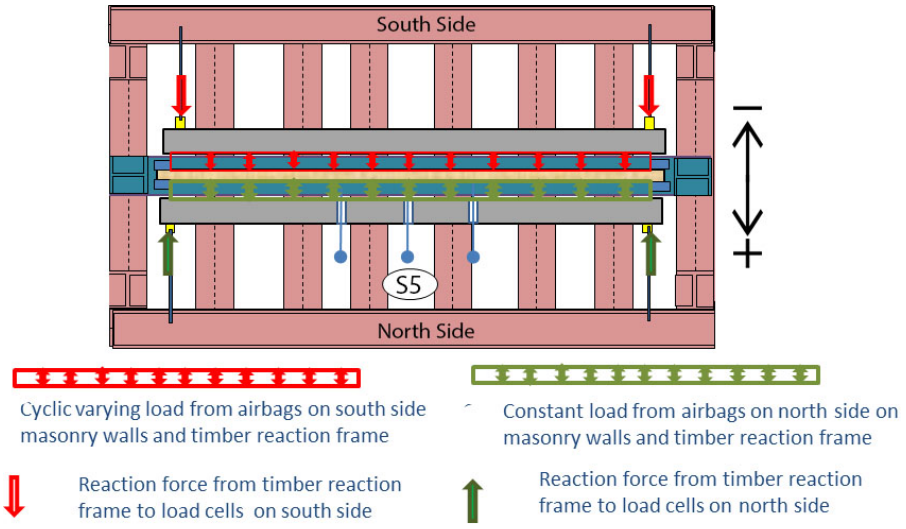

Figure 10 – Loading scheme for the application of lateral load in the out-of-plane test.

During the testing campaign, an asymmetric response of the wall was recorded in the lateral force versus mid-point displacement (capacity curve); in particular larger forces were recorded for positive displacements. This feature is the results of the adopted loading procedure in which the airbags on both sides of the wall are always inflated. By following the aforementioned loading procedure, a stable control of the imposed displacement can be achieved and sudden instability deformations of the wall are prevented. However, when the wall is subject to bending deformation, the airbag pressure is acting both on the compressive and tension side of the wall. In a deformed state of the wall, the friction between the wall and the airbags on the tension side of the wall can promote an increase in lateral force. This effect results larger for displacement in the positive loading direction, because the pressure in the airbags on the North side is higher. To illustrate the phenomena, Figure 11 shows a wall constant pressure of 70 mbar on the passive side (North side). For a positive displacement, the pressure in the airbag on the tension side of the wall will be equal to the initial constant pressure (70 mbar), while for negative displacements, the pressure in the airbag on the tension side of the wall will be lower (16 mbar). Consequently, the increase in lateral force is higher for positive displacements. This can explain the asymmetric behaviour recorded in the capacity curves.

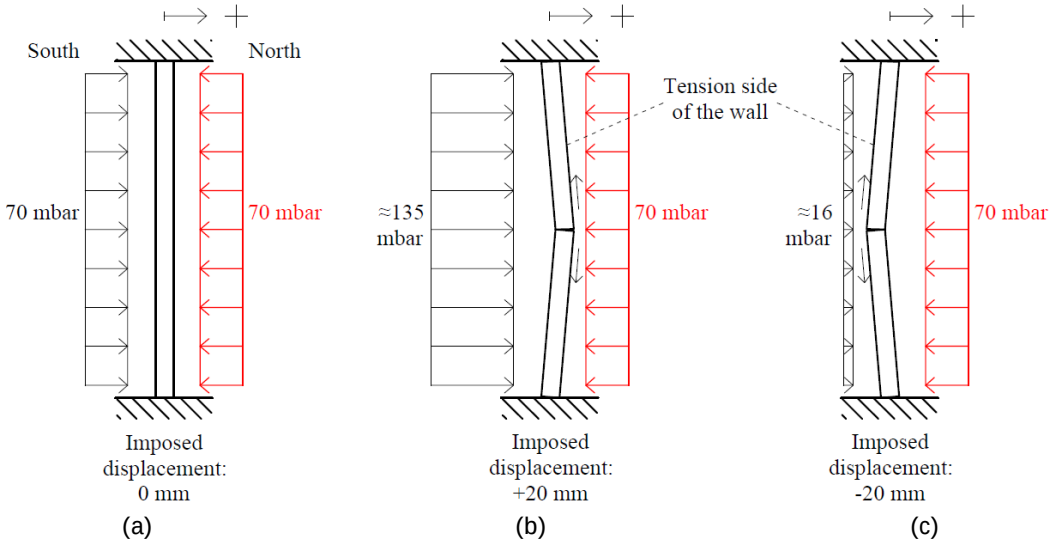

Figure 11 – Example of airbag pressure during the test on wall TUD_COMP-28 at cycle 10 (Initial constant pressure on the North side equal to 70mbar).

In order to evaluate the lateral force increment due to the adopted loading scheme, two quasi-static monotonic tests have been performed on the specimen TUD_COMP-27 after the standard testing procedure was applied (thus after that the wall was damaged in the cyclic test). The two monotonic tests adopted the following testing procedure:

- Standard loading procedure: the airbags on the North side were inflated till 170 mbar and subsequently the quasi-static monotonic test in displacement control was performed.
- Modified loading procedure: the airbags on the North side were completely deflated (0 mbar) and subsequently the quasi-static monotonic test in displacement control was performed.

The force-displacement curves of both tests are presented in Figure 12a. For displacement lower than a critical value d_{CR} (36.8 mm), no difference can be observed in the capacity curve obtained adopting the standard and modified loading procedure. By approximating the capacity curve obtained by the monotonic test with a bilinear expression, the increment in lateral force can be estimated as the force difference between the curves obtained using the standard and the modified loading procedure (Figure 12b):

$$\Delta F_{f,M27} = \begin{cases} 0 & d \le d_{CR,M27} \\ 0.2553 \cdot d - 9.396 & d > d_{CR,M27} \end{cases} \quad (1)$$

where $\Delta F_{f,M27}$ is the increment in lateral force given by friction between the wall and the airbags on the constant pressure side in the monotonic test, d is the mid-height displacement and $d_{CR,M27}$ is the critical mid-height displacement in the monotonic test for wall TUD_COMP-27 at which the increment in lateral force is higher than zero ($d_{CR,M27}$ = 36.8 mm).

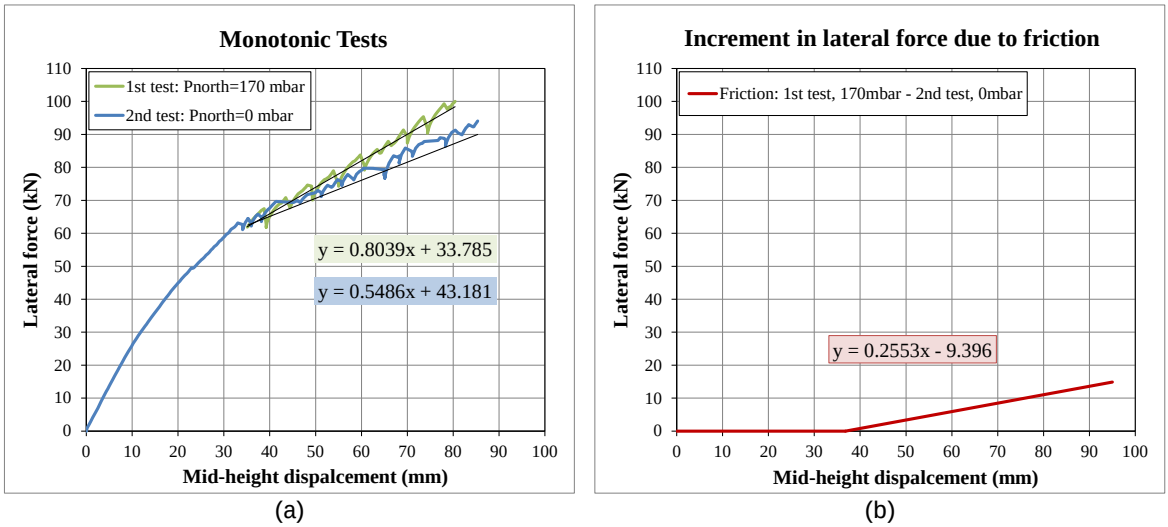

(a) (b)

Figure 12 – Monotonic test: (a) force-displacement curves; (b) increment in lateral force due to friction.

The envelope curve for positive displacement obtained by the cyclic test was corrected following Eq. (1). The envelope curve is determined as the "the locus of extremities of the load-displacement hysteresis loops, which contains the peak loads from the first" run "of each phase of the cyclic loading and neglects points on the hysteresis loops where the absolute value of the displacement at the peak load is less than that in the previous phase" [5]. In Figure 13, the black and green continuous lines show, respectively, the positive and negative envelope curves recorded during the cyclic test, while the dashed line shows the corrected capacity curve using Eq. (1) . By comparing the corrected envelope curve for positive displacements (dashed black line) and the recorded envelope curve for negative displacements (green line), a difference can still be noted. This difference can be related to the damage initiation, being the load first applied in the positive loading direction; consequently it can be assumed that while negative displacements are imposed the wall was previously damaged.

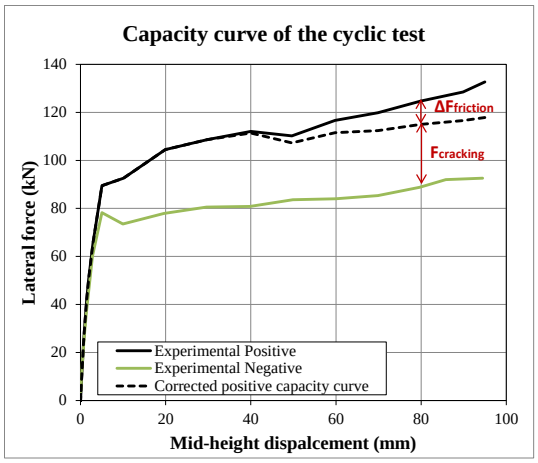

Figure 13 – Cyclic test on TUD_COMP-27 related to friction.

In order to obtain the corrected envelope curve for the other tests, the expression in Eq. (1), determined for the monotonic test on wall TUD_COMP-27, is modified accounting for the different specimen dimensions and testing conditions:

$$\Delta F_f^i = \begin{cases} 0 & d \le d_{CR,M27} \cdot t_w^i / t_{,M27} \\ \left[0.2553 \cdot \left(d \cdot \frac{t_{w,M27}}{t_w^i} \right) - 9.396 \right] \cdot \frac{p^i}{p_{M27}} & d > d_{CR,M27} \cdot t_w^i / t_{M27} \end{cases} \quad (2)$$

where ΔF_f^i is the increment in lateral force given by the friction between the wall and the airbags on the passive side for the *i*-th test, t_{M27} and t^i are respectively the wall thickness of the reference wall TUD_COMP-27 and of the *i*-th wall under consideration, p_{M27} and p^i are respectively the constant pressure in the airbag on the passive side for the reference monotonic test on wall TUD_COMP-27 and for the *i*-th wall under consideration and $d_{CR,M7}$ is the critical displacement evaluated for the reference test and equal to 36.8 mm. It is reasonable to assume that the correction proposed in Eq. (2) can only be applied to the two-way bending tests on squat walls for which the geometry, the boundary conditions and the crack pattern are comparable. Consequently, the correction is not applied to the one-way bending test (wall TUD_COMP-28). The parameters influencing Eq. (2) are summarised in Table 7 and a plot of the increment in lateral force is shown in Figure 14.

The increment in lateral force given by the friction between the wall and the airbags on the passive side for wall TUD_COMP-27 is estimated as:

$$\Delta F_f^{27} = \begin{cases} 0 & d \le 36.8mm \\ 0.2253 \cdot d - 8.2906 & 36.8mm < d \le 90mm \\ 0.2553 \cdot d - 9.3960 & d > 90mm \end{cases} \quad (3)$$

The increment in lateral force given by the friction between the wall and the airbags on the passive side for wall TUD_COMP-26 is estimated as:

$$\Delta F_f^{26} = \begin{cases} 0 & d \le 17.5mm \\ 0.2208 \cdot d - 3.8689 & d > 17.5mm \end{cases} \quad (4)$$

Table 7 – Parameters influencing the friction equation: specimen dimensions and testing conditions

Test	Wall thickness (t_w)	North side Airbag Pressure (p)
Monotonic test TUD_COMP-27	210 mm	170 mbar
Cyclic test on TUD_COMP-27	210 mm	100 mbar till 30 mm of displacement, 150 mbar between 30 and 90 mm, 170 mbar up to 90 mm.
Cyclic test on TUD_COMP-26	100 mm	70 mbar

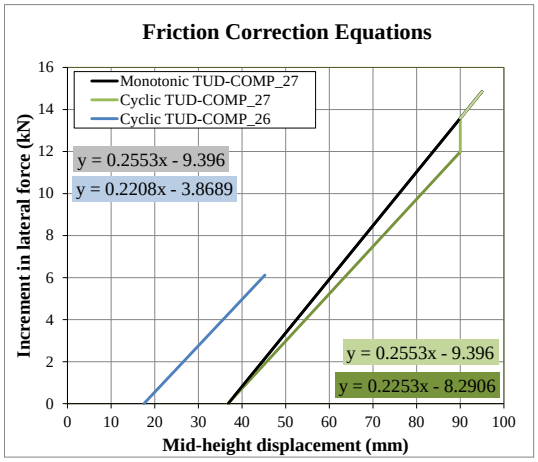

Figure 14 – Friction correction equation for cyclic tests on TUD_COMP-26 and 27.

6 Experimental results

In this Section, the experimental results of quasi-static out-of-plane cyclic tests are reported in terms of capacity curve (lateral force versus mid-point displacement), initial stiffness, displacement profile of the wall and crack pattern at the end of the test. The capacity curve has been corrected, following the procedure explained in Section 5.3, to account for the influence of a constant pressure in the airbags on the north side.

6.1 Solid clay brick masonry walls

Two walls made of solid clay brick masonry were tested: one wall in single wythe masonry (TUD_COMP-26) and one wall in double wythe masonry (TUD_COMP-27). In both cases the two-way out-of-plane bending failure mechanism was investigated.

6.1.1 Wall TUD_COMP-26

The wall TUD_COMP-26 in single wythe solid clay brick masonry was tested to investigate the two-way out-of-plane failure mechanism. A pre-compression load of 0.06 MPa was applied. Table 8 shows the loading scheme applied to wall TUD_COMP-26.

Table 8 - Loading scheme for wall TUD_COMP-26.

Cycle	Mid-point displacement	Mid-point displacement thickness ratio	Rate
	mm	%	mm/s
1	0.10	0.1	0.0018
2	0.20	0.2	0.0036
3	0.50	0.5	0.0090
4	0.70	0.7	0.0120
5	1.00	1.0	0.0180
6	1.50	1.5	0.0270
7	2.00	2.0	0.0360
8	3.00	3.0	0.0540
9	5.00	5.0	0.0900
10	10.00	10.0	0.1800
11	20.00	20.0	0.3600
12	30.00	30.0	0.5000
13	40.00	40.0	0.5000
14	50.00	50.0	0.5000
15	60.00	60.0	0.7500
16	70.00	70.0	1.0000
17	80.00	80.0	1.0000
18	90.00	90.0	1.0000
19	95.00	95.0	1.0000

Figure 15 shows the out-of-plane behaviour of the wall TUD_COMP-26 in terms of capacity curve. For the positive loading direction the envelope curve has been corrected following Eq. (4) (red line in Figure 15b). By comparing the corrected envelope curve for the positive displacement and the envelope curve for the negative displacement, a good agreement is found. During cycle 13 (u =±40 mm), the wall TUD_COMP-26 showed a maximum lateral force of +37.1 and -36.1 kN in the positive and negative loading direction, respectively (corrected envelope curve). The maximum lateral force, obtained with reference to the correlated envelope curve, is slightly higher in the positive loading direction. This can be linked to the damage evolution which occurs first in the positive loading direction, being this the first loading direction in every cycle. After the maximum lateral force was reached, a slightly reduction in force was observed in both loading directions. A maximum reduction of the lateral force equal to 40 and 25% in the positive and negative loading direction, respectively, was obtained in cycle 19 (u =±95 mm).

Figure 16 shows the initial stiffness K_{in}=*9.6 kN/mm* obtained experimentally as the linear regression of the lateral force – mid-point displacement curve of the first cycle, in the elastic phase. The specimen showed an almost linear-elastic behaviour for the first four cycles, up to a displacement of 0.7 mm and a lateral force of 6.5 kN.

Figure 17 and Figure 18 show the final crack pattern for the North and South side, respectively. The crack pattern can be summarised as following:

- Horizontal cracks formed at the first and last mortar bed joint
- Two main diagonal step-wise cracks developed starting from the corners and orientated towards the central part of the wall (red line in Figure 17a and Figure 18a). They had an average crack opening of 5 mm at the end of the test. Along these cracks an out-of-plane sliding displacement occurred as shown in Figure 18d,e.
- Secondary diagonal step-wise cracks occurred (blue line in Figure 17a and Figure 18a). They had an average crack opening of 0.5 mm at the end of the test.
- Splitting cracks in the thickness of the first and last course of bricks occurred (Figure 17e). This can be caused by the high stress concentration at the aforementioned locations for large mid-point displacements.

Figure 19 shows the fluctuation of the reaction force on the passive side, highlighting the development of the cracks during the test. It can be considered that the fluctuation observed for displacements higher than 20 mm (run 60, cycle 11) is an indication that the main cracks are opened.

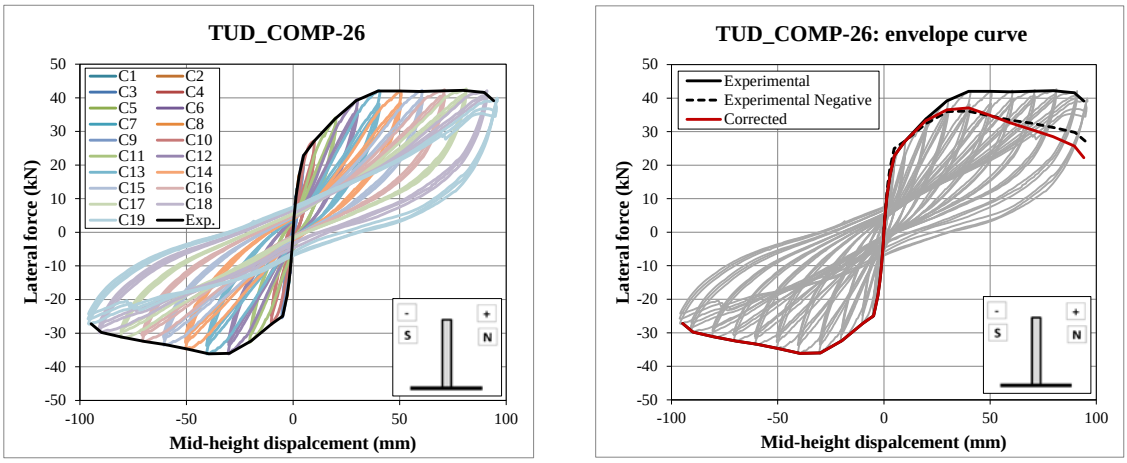

(a) (b)

Figure 15 – Capacity curve for wall TUD_COMP-26: (a) per cycle; (b) with corrected envelope curve.

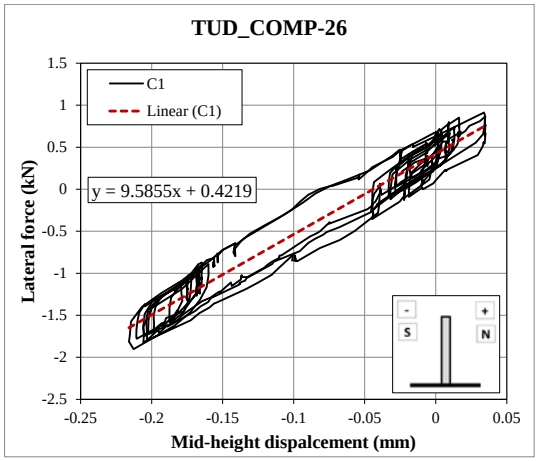

Figure 16 –Initial stiffness of the wall TUD_COMP-26.

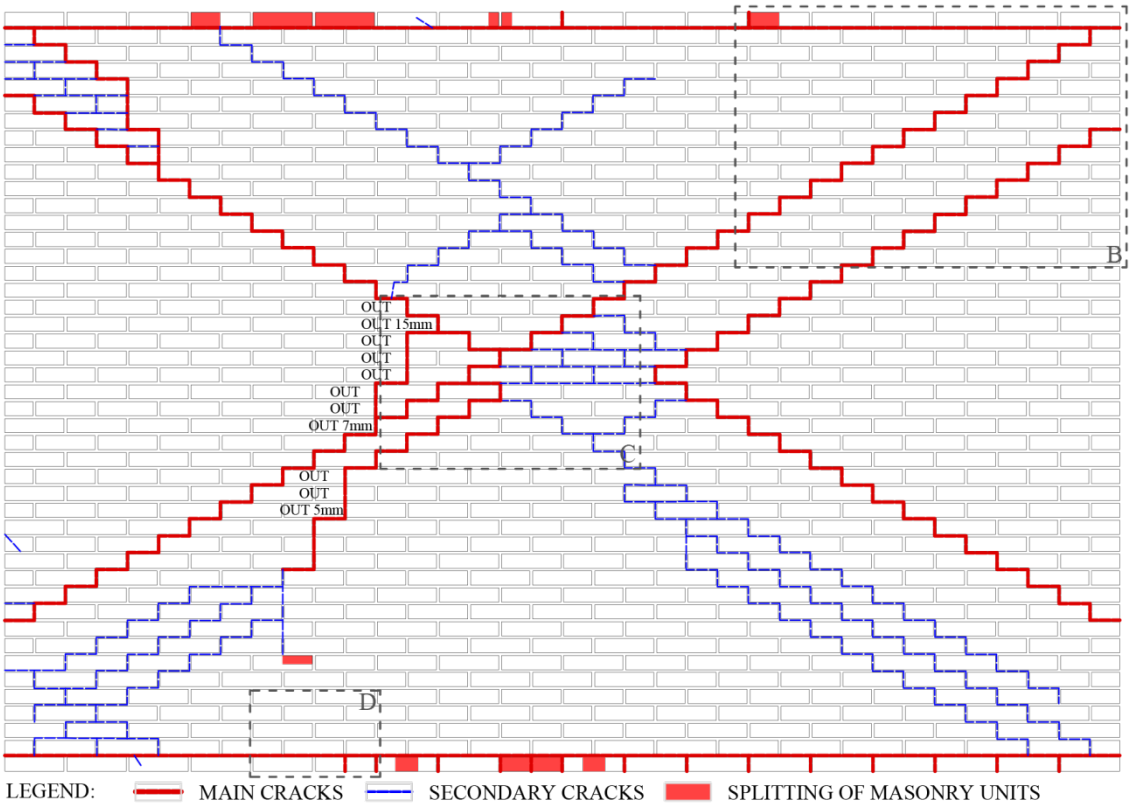

(a)

(b)

(c)

(d)

(e)

Figure 17 – Crack pattern on the North side: (a) overview; (b) diagonal cracks; (c) diagonal crack top right corner; (d) out-of-plane sliding (marked as "OUT" in figure a); (e) splitting of the bricks in the bottom row.

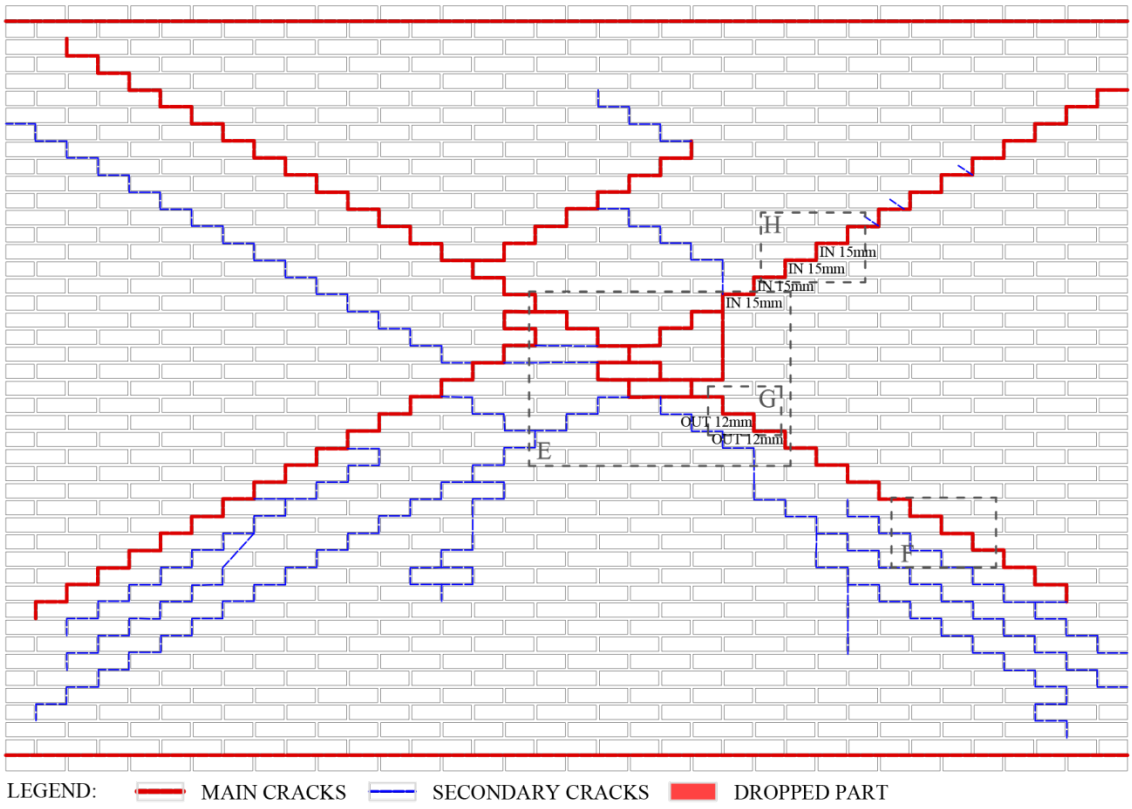

(a)

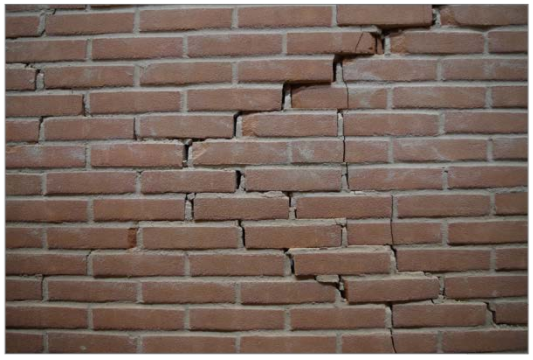

(b)

(c)

(d)

(e)

Figure 18 – Crack pattern on the South side: (a) overview; (b) diagonal cracks; (c) in-plane sliding; (d) out-of-plane sliding (referred as “OUT” in figure a); (e) out-of-plane sliding (marked as “IN” in figure a).

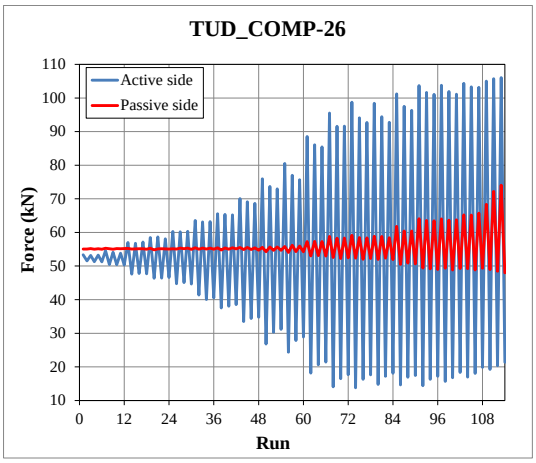

Figure 19 – Total force measured on the active (South) and passive (North) side.

6.1.2 Wall TUD_COMP-27

The wall TUD_COMP-27 in double wythe solid clay brick masonry was tested to investigate the two-way out-of-plane failure mechanism. A pre-compression load of 0.06 MPa was applied.
Table 9 shows the loading scheme applied to wall TUD_COMP-27. During the test the value of the constant pressure on the passive side was different: until cycle 8 (u = +/-3 mm) a pressure of 100 mbar was applied, from cycle 8 to cycle 19 (u =±90 mm) a pressure of 150 mbar was applied an in cycle 20 (u =±90 mm) a pressure of 170 mbar was applied. To exclude any influence of the change in value of the constant pressure, the same mid-height displacement was applied in cycle 8 and 9.

Table 9 - Loading scheme for wall TUD_COMP-27

Cycle	Mid-point displacement	Mid-point displacement thickness ratio	Rate	Pressure on the passive side
	mm	%	mm/s	mbar
1	0.10	0.05	0.0018	100
2	0.20	0.1	0.0036	100
3	0.50	0.2	0.0090	100
4	0.70	0.3	0.0120	100
5	1.00	0.5	0.0180	100
6	1.50	0.7	0.0270	100
7	2.00	1.0	0.0360	100
8	3.00	1.4	0.0540	100
9	3.00	1.4	0.0540	150
10	5.00	2.4	0.0900	150
11	10.00	4.8	0.1800	150
12	20.00	9.5	0.3600	150
13	30.00	14.3	0.3600	150
14	40.00	19.0	0.3600	150
15	50.00	23.8	0.3600	150
16	60.00	28.6	0.3600	150
17	70.00	33.3	0.3600	150
18	80.00	38.1	0.3600	150
19	90.00	42.9	0.3600	170
20	95.00	45.2	0.3600	170

Figure 20 shows the out-of-plane behaviour of the wall TUD_COMP-27 in terms of capacity curve. For the positive loading direction the envelope curve has been corrected following Eq. (3) (red line in Figure 20b). By comparing the corrected envelope curve for the positive displacement and the envelope curve for the negative displacement a similar trend and a good agreement is found.
In cycle 10 (u =±5 mm), the wall TUD_COMP-27 showed a maximum lateral force of +89.5 kN and -78.3 kN in the positive and negative loading direction, respectively. After this cycle, an increase in lateral force was observed both in the negative and positive loading direction. In cycle 20 (u =±95 mm), in which the wall is subject to a mid-point displacement equal to half of the wall thickness, a maximum increase in force of 32% is reached with reference to the corrected envelope curve. In this test the influence of damage evolution on the basis of the loading direction is more evident than for the wall TUD_COMP-26; this may be caused by the difference in wall thickness (210 mm for wall TUD_COMP-27 and 100 mm for wall TUD_COMP-26).

Figure 21 shows the initial stiffness K_{in}*= 41.4 kN/mm* obtained experimentally as the linear regression of the lateral force – mid-height displacement curve of the first cycle, in the elastic phase. Considering the first two cycles (u = +/- 0.1 mm and u = +/- 0.2 mm) a reduction of 9.7% of the stiffness is observed. This reduction is higher than the one observed during the test on wall TUD_COMP-26 equal to 2.1%.

Figure 22 and Figure 23 show the final crack pattern for the North and South side, respectively. The crack pattern can be summarised as following:

- Horizontal cracks formed at the first and last mortar bed joint.
- Two main diagonal step- wise cracks developed starting from the corners and orientated towards the central part of the wall (red line in Figure 22a and Figure 23a). They had an average crack opening of 15 mm at the end of the test. Along these cracks an out-of-plane sliding displacement occurred as shown in Figure 22d.
- Secondary diagonal step-wise cracks occurred (blue line in Figure 22a and Figure 23a). They had an average crack opening of 0.5 mm at the end of the test.
- One horizontal crack at the centre of the wall occurred from which all the diagonal cracks bifurcate (Figure 22c and Figure 23c).

The splitting of the bricks in the bottom and top row and a general damage of the units along all the diagonal and horizontal cracks can be observed in both side of the wall as shown in Figure 22b,d and Figure 23b,d,e.

Figure 24 shows the fluctuation of the reaction force on the passive side, highlighting the gradual development of the cracks during the test.

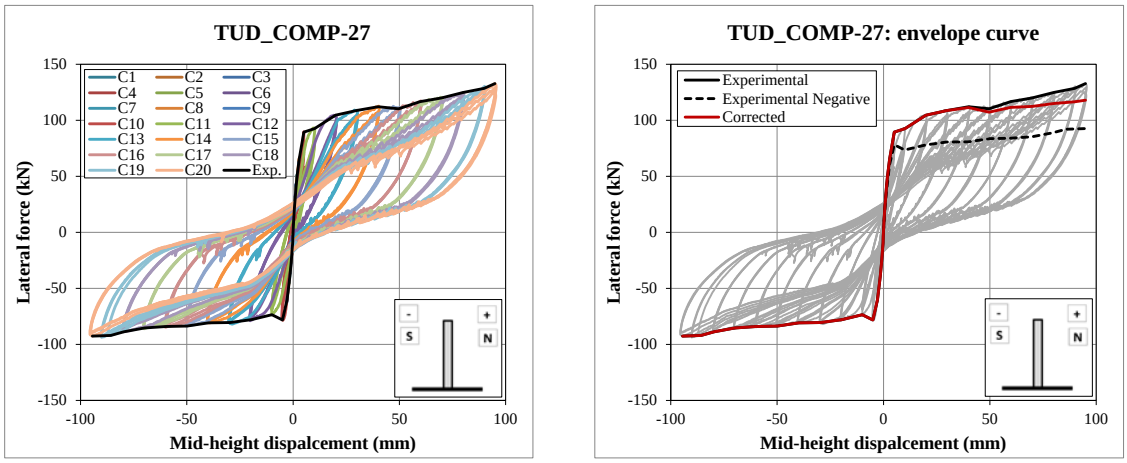

(a) (b)

Figure 20 – Capacity curve for wall TUD_COMP-27: (a) per cycle; (b) with corrected envelope curve.

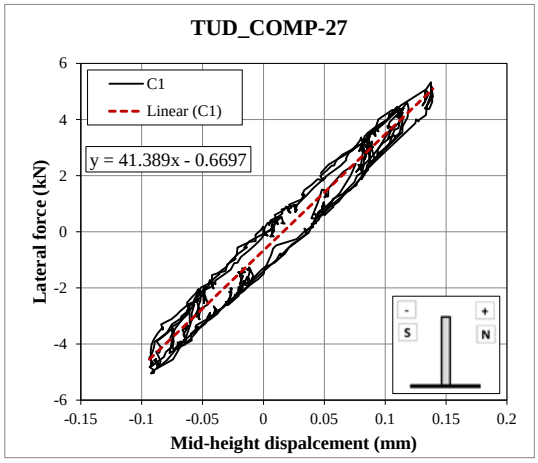

Figure 21 –Initial stiffness of the wall TUD_COMP-27.

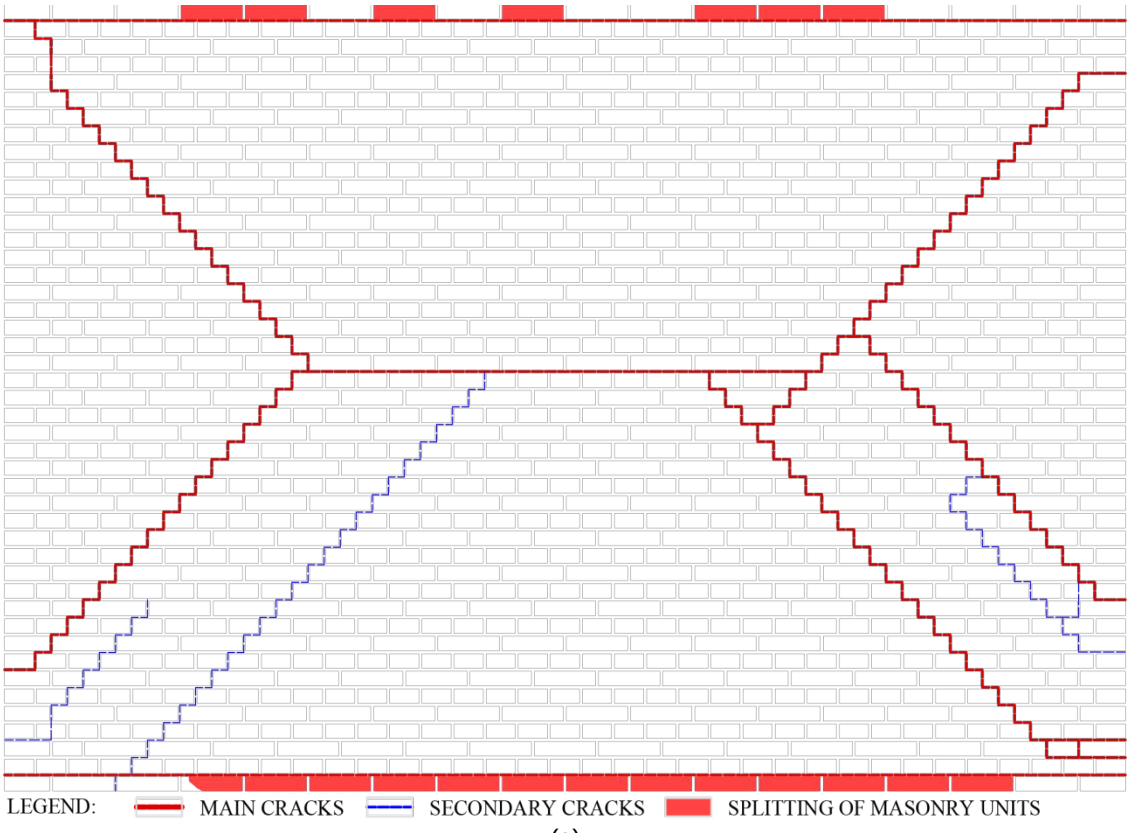

(a)

(b)

(c)

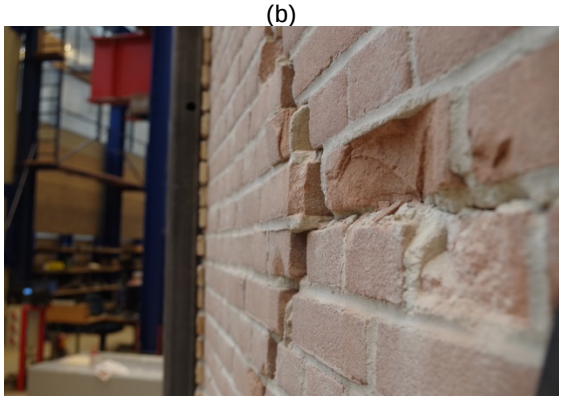

(d)

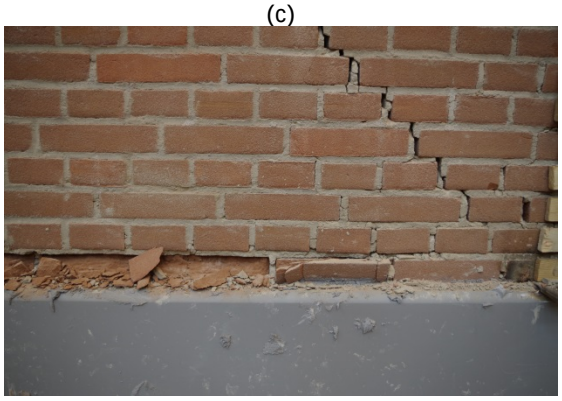

(e)

Figure 22 – Crack pattern on the North side: (a) overview; (b) main and secondary diagonal cracks; (c) horizontal crack; (d) out-of-plane sliding; (e) splitting of the bricks in the bottom row.

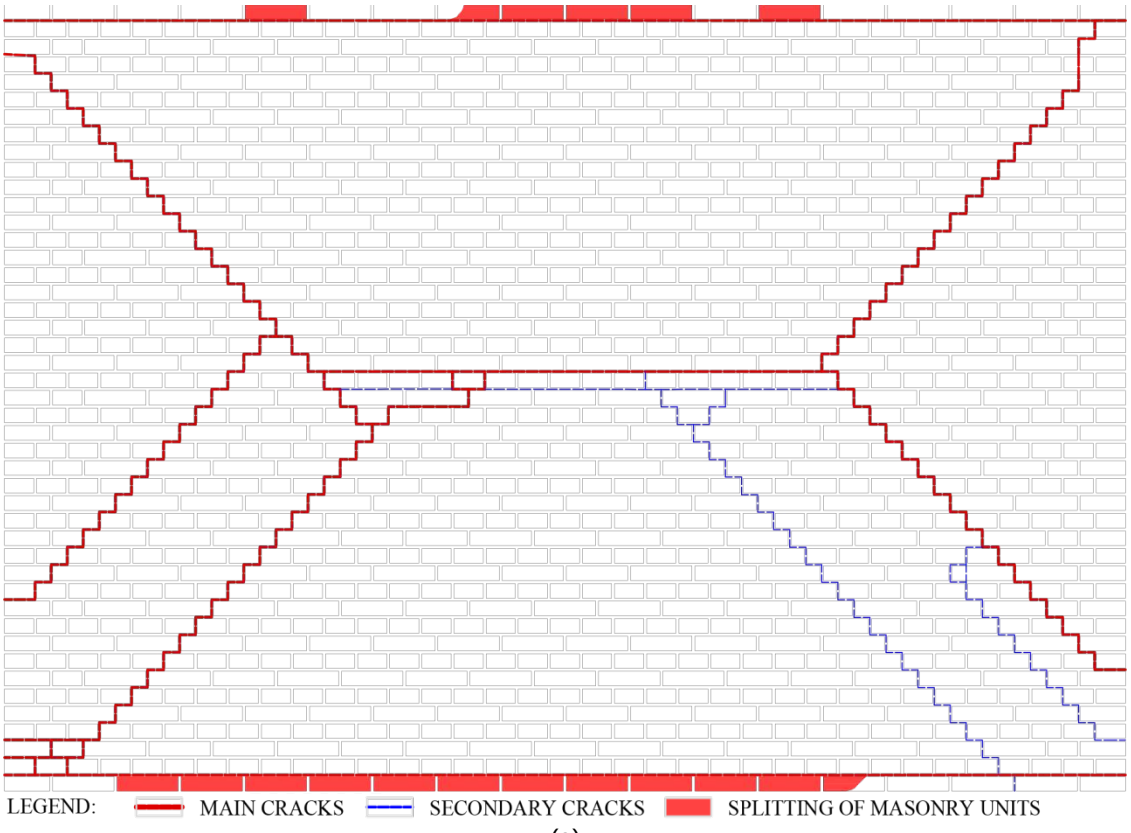

(a)

(b)

(c)

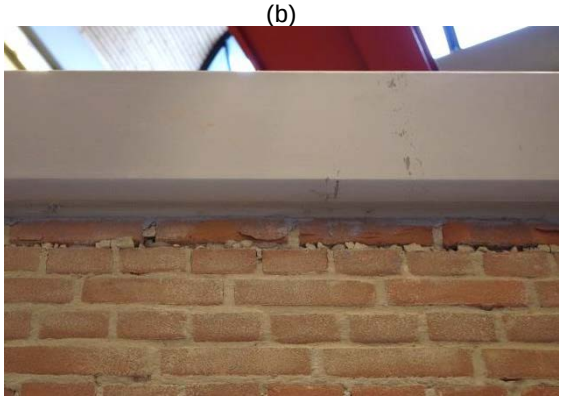

(d)

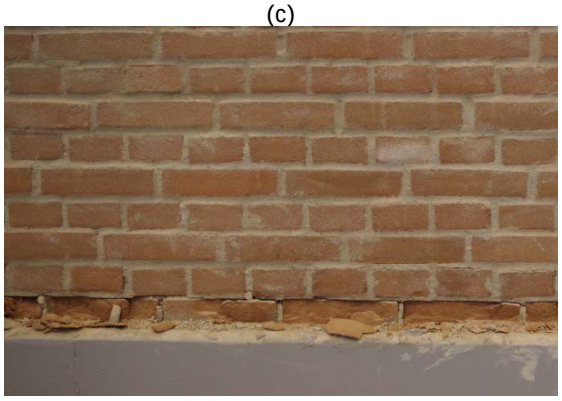

(e)

Figure 23 – Crack pattern on the South side: (a) overview; (b) diagonal cracks; (c) horizontal crack; (d) damage of the bricks in the top row; (e) splitting of the bricks in the bottom row.

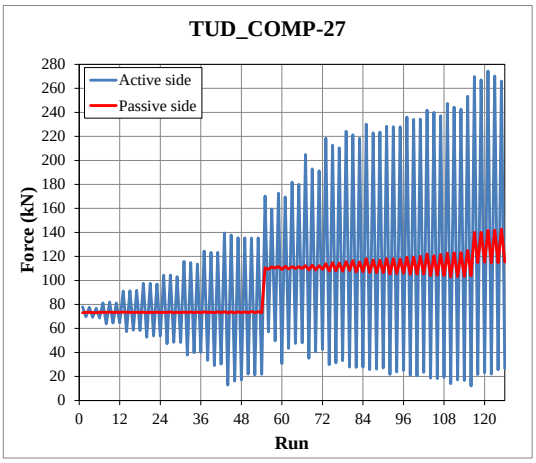

Figure 24 –Total force measured on the active (South) and passive (North) side.

6.2 Calcium silicate element masonry walls

Two walls made of calcium silicate element masonry were tested to investigate the one-way and two-way out-of-plane bending failure mechanism, respectively (TUD_COMP-28 and TUD_COMP-29).

6.2.1 Wall TUD_COMP-28

The wall TUD_COMP-28 in calcium silicate element masonry was tested to investigate the one-way out-of-plane failure mechanism. A pre-compression load of 0.25 MPa was applied.
Table 10 shows the loading scheme applied to wall TUD_COMP-28.

Table 10 - Loading scheme for wall TUD_COMP-28

Cycle	Mid-point displacement	Mid-point displacement thickness ratio	Rate
	mm	%	mm/s
1	0.20	0.17	0.0036
2	0.50	0.42	0.0090
3	0.70	0.58	0.0150
4	1.00	0.83	0.0180
5	1.50	1.25	0.0270
6	2.00	1.67	0.0360
7	3.00	2.50	0.0540
8	5.00	4.17	0.0900
9	10.00	8.33	0.1000
10	20.00	16.67	0.1000
11	40.00	33.33	0.2000
12	60.00	50.00	0.3000
13	80.00	66.67	0.4000
14	98.00	81.67	0.5000
15	98.00	81.67	0.5000

Figure 25 shows the out-of-plane behaviour of the wall TUD_COMP-28 in terms of capacity curve. The difference between positive and negative envelope curve in terms of lateral force can be related to the effect of the constant pressure on the tension side of the wall during the test, as described in Section 5.3. Due to the differences in geometry, boundary conditions and crack pattern between the one-way and two-way bending test, the correction procedure described in Section 5.3 cannot be applied. It is suggested to consider the capacity curve for negative displacement as representative for the wall behaviour.
During cycles 9 and 10 (u =±10 mm and u =±20 mm), the wall TUD_COMP-28 showed a maximum lateral force of -18.0 kN in negative loading direction. After the maximum lateral force was reached, a reduction in force was observed. During cycle 14 (u=+98 mm), a local peak can be observed for the positive loading direction. This is caused by the clipping of the airbag on the passive side within the horizontal crack at mid-height of the wall.

Figure 26 shows the initial stiffness K_{in}*=12.3 kN/mm* obtained experimentally as the linear regression of the lateral force–mid-point displacement curve of the first cycle, in the elastic phase. The specimen denoted an elastic behaviour for the first three cycles, up to a displacement of 0.7 mm and a lateral force of 8.2 kN.

Figure 27 shows the evolution in crack opening for each bed joint. It is measured along the thickness of the wall on the east side of the all. It should be pointed out that this is a local measurement, which can provide an indication of the crack opening. Due to the presence of the airbags the crack pattern on the face of the wall cannot be monitored. The first crack opening higher than 0.01 mm was registered at imposed displacement of 1 mm by CR5Z sensor, at the bottom of the wall (Figure 27b and Figure 27c). The recorded lateral force at onset of cracking is 10.0 kN. The second crack, measured at the mid-height by sensor CR3N (Figure 27d), appeared at imposed displacement of 1.5 mm (Figure 27b). The third crack, registered by CR1Z sensor at the top of the wall, appeared at imposed displacement of 10 mm. The maximum crack opening recorded at the top mid-height and bottom bed joint is respectively 6.7 mm, 13.1 mm and 6.0 mm.

Figure 28 shows the final crack pattern of the wall TUD_COMP-28. After the test, three horizontal cracks located at the bottom, mid-height and top bed joint can be observed. In correspondence of the three horizontal cracks damage in the calcium silicate elements and in the kicker layers is observed (Figure 28b,c). This gives an indication of the stress localisation in these areas due to the rotation of the two portions of the wall.
Figure 29 shows the fluctuation of the reaction force on the passive side, highlighting the development of the cracks during the test. The fluctuation observed for displacements higher than 10 mm confirms the fact that all 3 main cracks are fully developed, as shown in Figure 27.

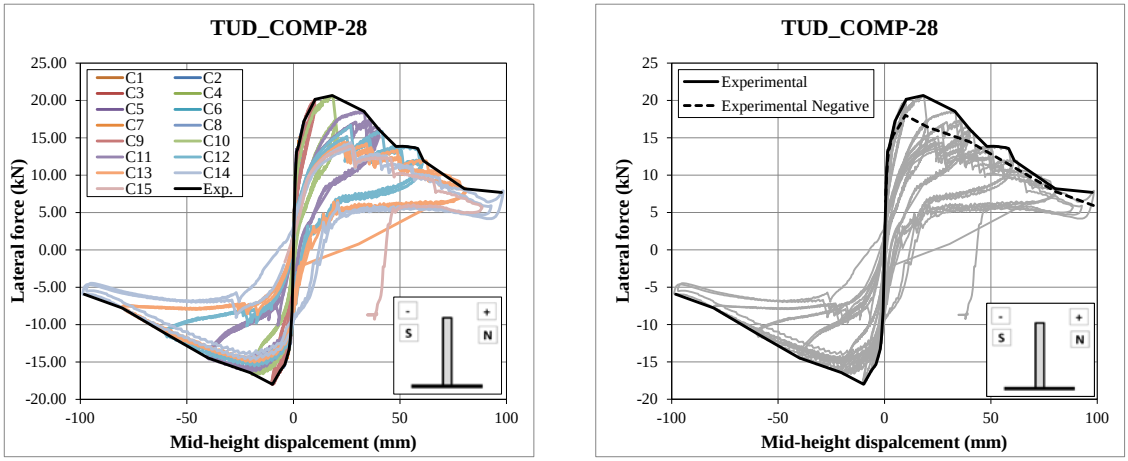

(a) (b)

Figure 25 – Capacity curve for wall TUD_COMP-28: (a) per cycles; (b) envelope curve.

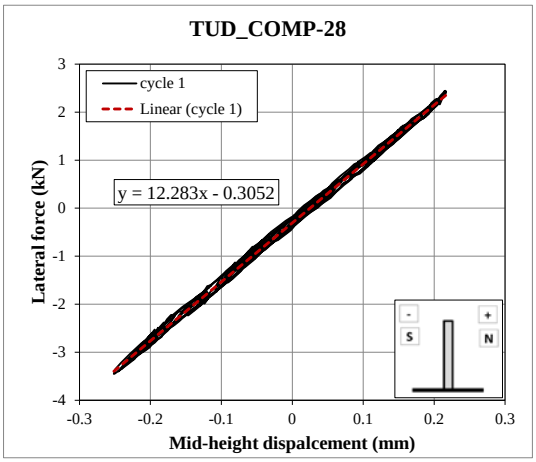

Figure 26 –Initial stiffness of the wall TUD_COMP-28.

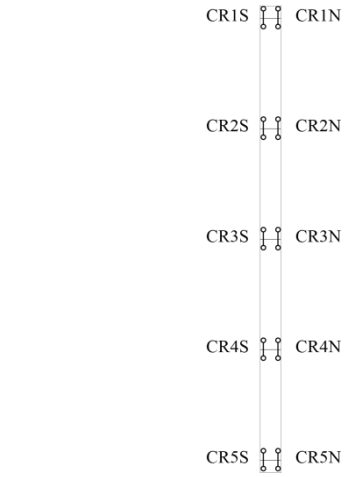

(a)

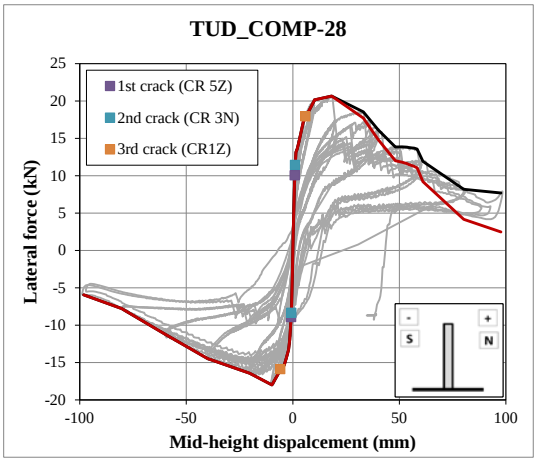

(b)

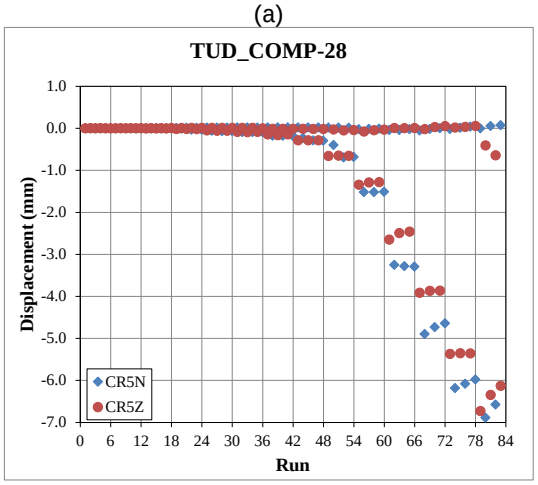

(c)

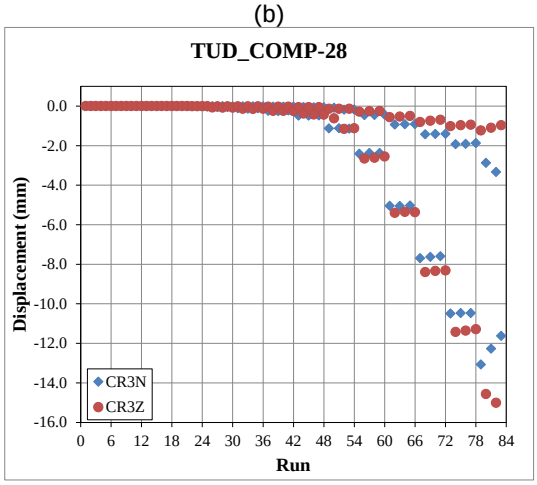

(d)

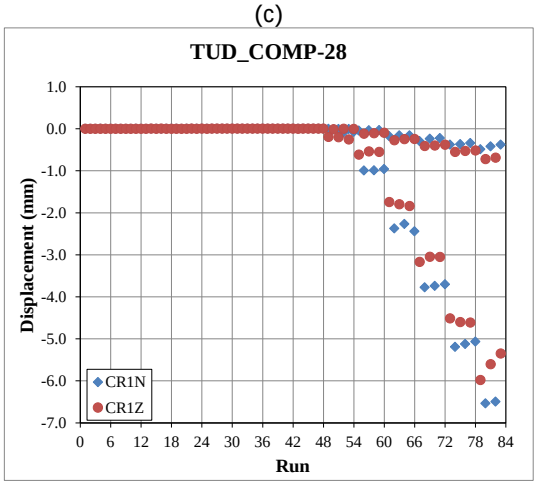

(e)

Figure 27 – Crack opening: (a) sensors position on the East side of the wall; (b) Cracking evolution; (c) crack at the bottom mortar bed joint; (d) crack at the mid-height mortar bed joint; (e) crack at the top mortar bed joint.

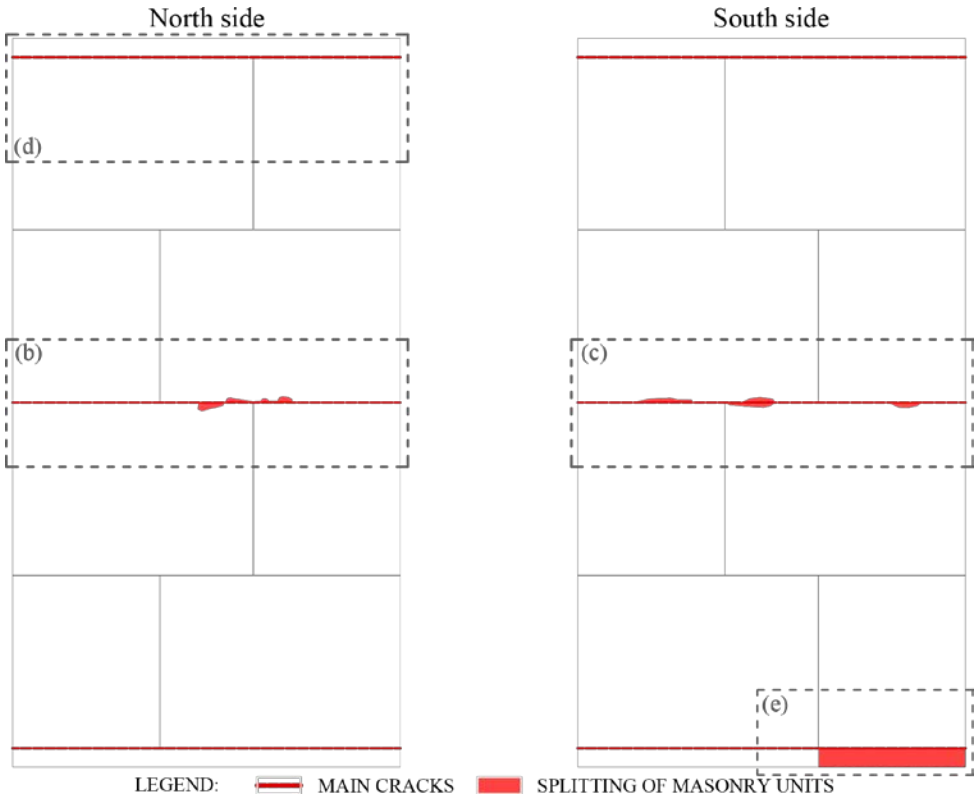

(a)

(b)

(c)

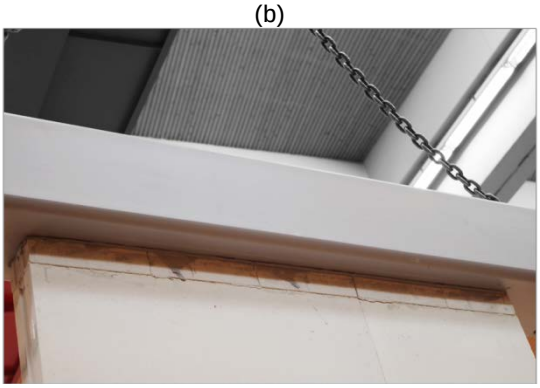

(d)

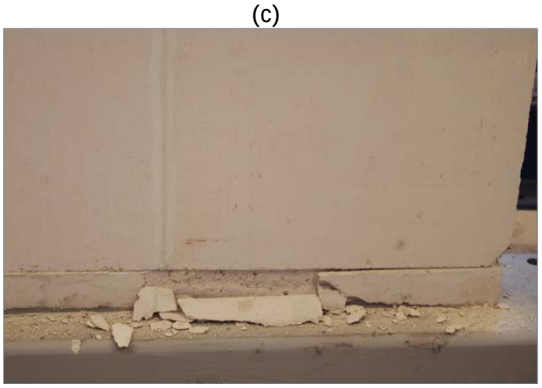

(e)

Figure 28 – Crack pattern TUD_COMP-28: (a) drawing; (b) mid-height crack North side; (c) mid-height crack South side; (d) top crack North side; (e) splitting of the bricks in the bottom South row.

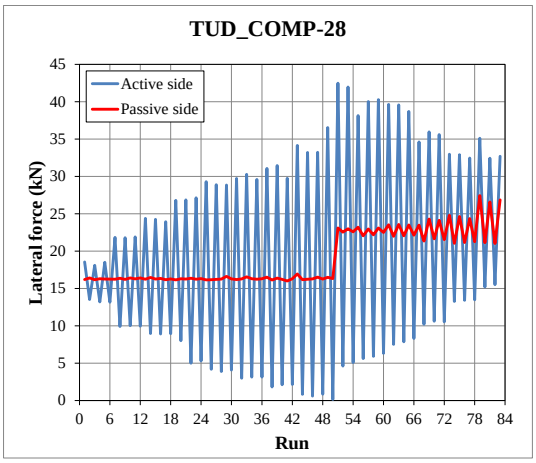

Figure 29 – Total force measured on the active (South) and passive (North) side.

6.2.2 Wall TUD_COMP-29

The wall TUD_COMP-29 in calcium silicate element masonry was tested to investigate the two-way out-of-plane failure mechanism. A pre-compression load of 0.06 MPa was applied.
Table 10 shows the loading scheme applied to wall TUD_COMP-29. Due to technical problems, the test was stopped prematurely and continuation of the test was not possible.

Table 11 - Loading scheme for wall TUD_COMP-29

Cycle	Mid-point displacement	Mid-point displacement thickness ratio	Rate
	mm	%	mm/s
1	0.10	0.08	0.0018
2	0.20	0.17	0.0036

Figure 30a shows the initial stiffness K_{in}=*15.9 kN/mm* obtained experimentally as the linear regression of the lateral force – mid-height displacement curve of the first cycle, in the elastic phase.

Due to the technical problems, a sudden application of the out-of-plane wall occurred after cycle 2 resulting in damage of the wall and of the equipment. Consequently, it is not possible to provide any information regarding the maximum lateral force of this wall. However, it is possible to note that the application of an out-of-plane load leads mainly to the formation of cracks at both the bed and head joints; limited damage it is observed in the element (Figure 30b). These observations should be only considered has an indication due to the incorrect load application.

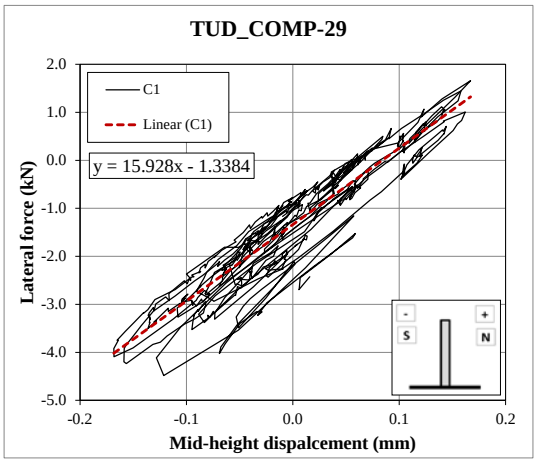

(a)

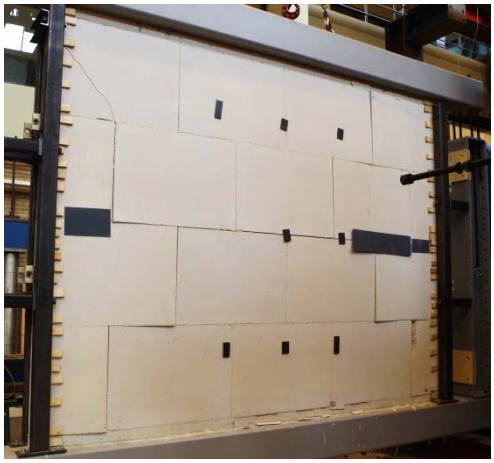

(b)

Figure 30 –Initial stiffness of the wall TUD_COMP-29.

7 Considerations on the initial stiffness

In this Section the experimental results in terms of the initial stiffness are compared with the analytical formulations. Remarks regarding the boundary conditions, previously presented in Section 5.1, are made.

7.1 One-way bending

Assuming an elastic behaviour of the wall in the initial phase, the initial stiffness is evaluated considering three different static schemes: double clamped, simply supported and clamped at the bottom side and hinged at top side. The formulae used for the calculations are:

$$K_{in} = \begin{cases} \frac{384}{5}\frac{EI}{H^3} \rightarrow Hinge - Hinge \\ \cong \frac{384}{2}\frac{EI}{H^3} \rightarrow Clamped - Hinge \\ 384\frac{EI}{H^3} \rightarrow Clamped - Clamped \end{cases} \quad (5)$$

The prediction of initial stiffness for the one-way bending test on wall TUD_COMP-28 is reported in Table 12. They are based on the elastic modulus of masonry in the direction perpendicular to bed joints evaluated between 1/10 and 1/3 of the maximum stress (E_3 in Table 2). By comparing the experimental and analytical results, it can be noticed that by assuming a clamped constraint at the bottom side and a hinged constraint at the top side, a good agreement between experimental and numerical results is observed.

Additional considerations on the boundary conditions can be made by analysing the displacement profile of the wall during the test. During the test the deformation of the wall has been measured at three locations over the height of the wall on both the left and right side. By taking the average of the displacements measured on the left and right side of the wall and relating the top and bottom displacements to the mid-height displacement, the displacement ratios shown in Figure 31a can be obtained. Figure 31a shows that in the first 3 cycles (up to run 18) the ratio between the top and mid-height displacement r_t is approximatively 0.78, while the ratio between the bottom and mid-height displacement r_b is approximatively 0.33. This displacement profile is in agreement with the one expected for a clamped-hinged static scheme (Figure 31c). After the opening of all three cracks (Figure 27b), which occurs at a displacement of ±10 mm (run 54, cycle 10), the displacement profile of the wall is in agreement with the one expected for the rigid-block scheme (Figure 31d).

Table 12 – Comparison between analytical and experimental results in terms of initial stiffness for wall TUD_COMP-28 subject to one-way bending.

Static scheme		**Initial stiffness K_{in} (kN/mm)**
Bottom constrain	**Top constrain**	
Clamped	Clamped	32.9
Clamped	Hinged	16.4
Hinged	Hinged	6.6
Experimental		12.3

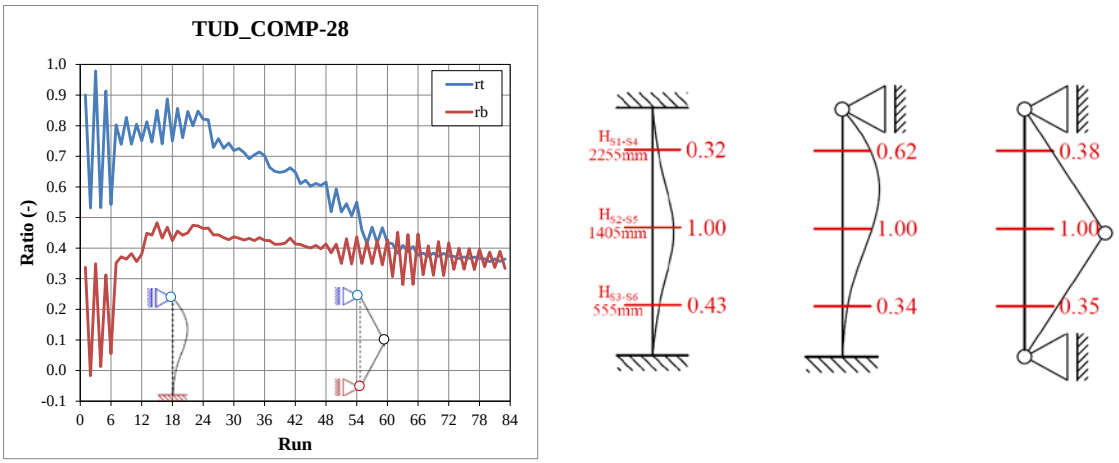

(a) (b) (c) (d)

Figure 31 – (a) Measured displacement ratio; (b) theoretical displacement ratio for clamped-clamped static scheme; (c) theoretical displacement ratio for fix-hinge static scheme; (d) theoretical displacement ratio for rigid block scheme.

7.2 Two-way bending

In the two-way out-of-plane bending test the wall is considered as a plate constrained on all four sides. The vertical sides are considered as hinges, while for the top and bottom sides different restraints are taken into account. Three different static schemes are considered: clamped at top and bottom side, hinged at top side and clamped at bottom side and hinged on all four sides. The first scheme is reported in Figure 32.

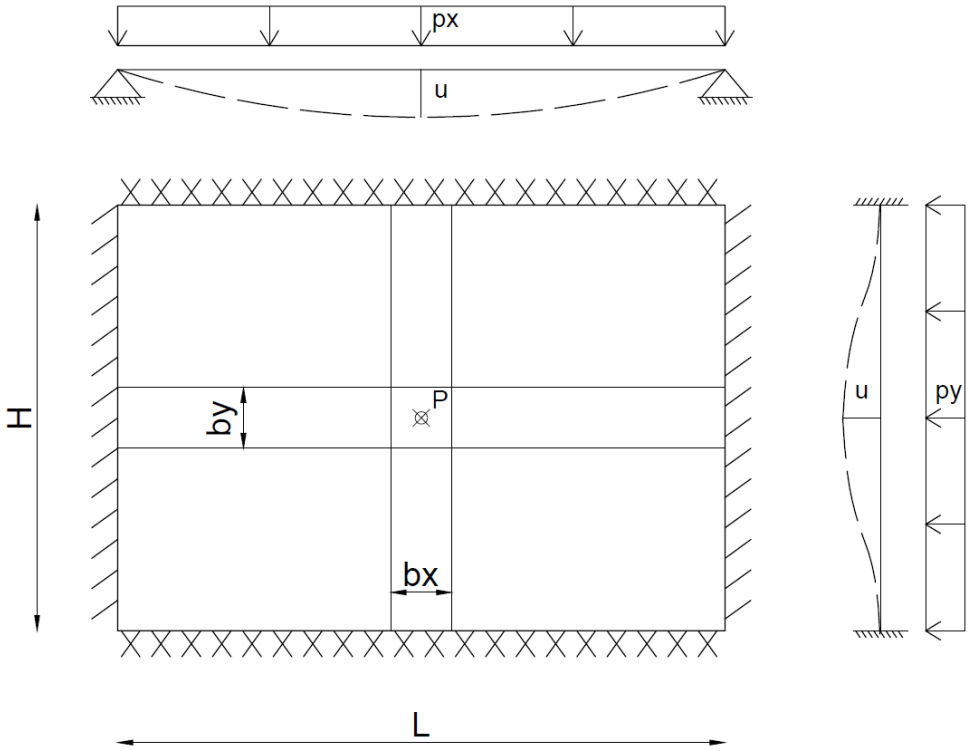

Figure 32 – Wall schematised as two beams, one spanning vertically and one spanning horizontally.

To calculate the initial stiffness, the wall is schematised as two beams: a beam spanning vertically from top to bottom (y-axis) and a beam spanning horizontally from left to right (x-axis). The uniform applied pressure p on the wall (Figure 32) can be redistributed to the two beams imposing that the displacement of the central point P is the same in the two configurations. Taking as example the static scheme shown in Figure 32, the equilibrium equations read:

$$\begin{cases} p_x + p_y = p \\ \frac{5}{384}\frac{p_x L^4}{EI} = \frac{1}{384}\frac{p_y H^4}{EI} \end{cases} \tag{6}$$

Being the beams' width (b_x and b_y) not important for the stiffness evaluation, a unitary value is considered and the modulus of inertia per unit of length ($I = t^3/12$) is used. The system can be solved for p_x and p_y as following:

$$\begin{cases} p_x = p\frac{H^4}{H^4 + 5L^4} \\ p_y = p\frac{5L^4}{H^4 + 5L^4} \end{cases} \tag{7}$$

The displacement at point P results:

$$u = \frac{5}{384}\, p\, \frac{H^4}{H^4 + 5L^4}\frac{L^4}{EI} \tag{8}$$

The initial stiffness of the wall can be calculated as followed:

$$K_{in} = \frac{384}{5}\frac{EI\left(H^4 + 5L^4\right)}{H^3L^3} \tag{9}$$

The same procedure is applied to the other static schemes and the corresponding equations results:

$$K_{in} = \begin{cases} \frac{384}{5}\frac{EI\left(H^4 + 5L^4\right)}{H^3L^3} \rightarrow & Clamped\ \ at\ \ the\ \ top\ \ and\ \ bottom - Hinged\ \ lateral\ \ sides \\ \frac{384}{5}\frac{EI\left(2H^4 + 5L^4\right)}{2H^3L^3} \rightarrow & Clamped\ \ at\ \ the\ \ bottom - Hinged\ \ other\ \ sides \\ \frac{384}{5}\frac{EI\left(H^4 + L^4\right)}{H^3L^3} \rightarrow & Hinged\ \ on\ \ all\ \ sides \end{cases} \tag{10}$$

Table 13 – Comparison between analytical and experimental results in terms of initial stiffness for wall TUD_COMP-26, TUD_COMP-27 and TUD_COMP-29 subject to in two-way bending.

Static scheme	**Initial stiffness K_{in} (kN/mm)**		
	TUD_COMP-26	**TUD_COMP-27**	**TUD_COM-29**
Clamped at top and bottom, hinged on the lateral sides	30.4	177.1	87.1
Clamped at the bottom, hinged on the other sides	15.9	92.7	46.2
Hinged on all sides	7.1	42.1	21.7
Experimental	9.6	41.4	15.9

Table 13 lists the analytical estimations of the stiffness for the three static schemes. The estimations are based on the elastic modulus of masonry in the direction perpendicular to bed joints evaluated between 1/10 and 1/3 of the maximum stress (E_3 in Table 2). The initial stiffness of the specimens TUD_COMP-26, TUD_COMP-27 and TUD_COMP-29 is respectively 9.6 kN/mm, 41.4 kN/mm and 15.9 kN/mm. By comparing the experimental and analytical results, it can be noticed that a good agreement between experimental and numerical results is obtained considering a static scheme with hinged supports at all sides of the wall.

Additional considerations on the boundary conditions can be made by analysing the displacement profile of the wall during the test. During the test the deformation of the wall has been measured at three locations over the height of the wall in the central zone (Figure 7b). By relating the top and bottom displacements to the mid-point displacement, the displacement ratios shown in Figure 33 can be obtained. Considering the wall TUD-COMP-26 (Figure 33a), the ratio r_t between the top displacement and the mid-point displacement is constant and equal to 0.64 between cycles 3 and 9. After cycle 11, the ratio r_t decreases to a value equal to 0.47, suggesting that for the first part of the test the horizontal crack close to the top edge was not opened. It should be mentioned that at the top of the wall a little play was recorded between the cross-beams and the external steel frame due to the glass plates (Figure 5), inserted to permit the vertical displacement of the wall and avoid friction between the cross-beams and the external steel frame. The ratio r_b between the displacement at the bottom and the mid-point displacement decreases from 0.47 to 0.37. The sudden decrease in both displacement ratios after cycle 11 (run 60) can be linked to the opening of the main diagonal and horizontal cracks, confirmed also by the fluctuation of the reaction force on the passive side (Figure 19). Figure 33b shows the displacement profile for the wall TUD_COMP-27. Similarly to TUD-COMP_26, during this test the ratio r_t decreases after cycle 9 from an approximatively constant value of 0.86 to 0.47 and the ratio r_b decreases from 0.43 to 0.37. The same considerations made for TUD-COMP_26 remain valid. It should be mentioned that in both walls the difference between the ratios r_t and r_b at the end of the test can be attributed to the position of the sensor with respect to the respect to the central crack; in both cases the mid-point sensor is below the horizontal crack.
The displacement profile for the wall TUD_COMP-29 is not available due premature failure of the test.

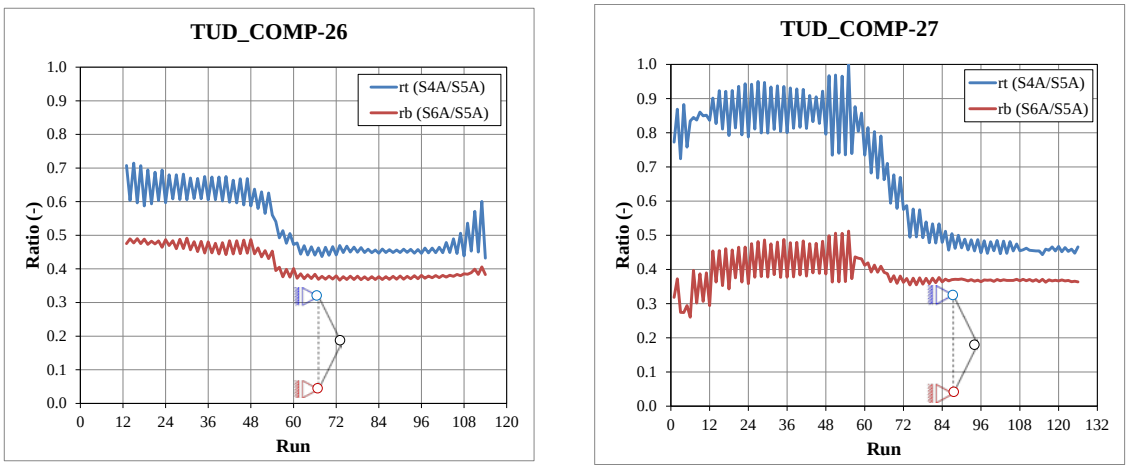

(a) (b)

Figure 33 –Measured displacement ratio S4/S5 and S6/S5: (a) TUD_COMP-26 and (b) TUD_COMP-27

8 Analytical calculations to estimate the lateral force

In this Section, the experimental results are compared with the rigid block model and with the analytical formulations by Australian standard [6] and Eurocode 6 [7]. The comparison is made in terms of maximum lateral force.

8.1 Estimation for one-way bending mechanism

The one-way out-of-plane failure mechanism is analysed via the kinematic limit analysis by assuming the rigid block mechanism shown in Figure 34. The model assumes the formation of three cracks located in the mortar bed joint at the top, bottom and mid-height of the wall. Considering the self-weight of the wall, the vertical pre-compression and the uniform lateral load, the total work can be written as:

$$\lambda(1-\beta)W\frac{u}{2}+\lambda\beta W\frac{u}{2}-W\frac{t_w}{2}\frac{u}{H_{eff}}-(1-\beta)W\frac{t_w}{2}\left(\frac{1}{\beta}+\frac{1}{2(1-\beta)}\right)\frac{2u}{H_{eff}}-N\frac{t_w}{2}\left(\frac{1}{\beta}+\frac{1}{1-\beta}\right)\frac{2u}{H_{eff}}=0 \quad (11)$$

where u is the horizontal displacement at mid-height of the wall, W is the self-weight of the wall, t_w is the wall thickness, N is the pre-compression load, λ is the self-weight multiplier, H_{eff} is the effective height of the wall and β is the crack height ratio.

Solving Eq. (11), the self-weight multiplier λ can be calculated as:

$$\lambda=\left(\frac{1}{\beta}+\frac{1}{\beta(1-\beta)}\frac{N}{W}\right)\cdot\left(\frac{t_w}{H_{eff}/2}\right) \quad (12)$$

The self-weight multiplier λ assumes is minimum value in the case of:

$$\beta=\left(\frac{N}{W}+1\right)-\sqrt{\frac{N}{W}\cdot\left(\frac{N}{W}+1\right)} \quad (13)$$

The lateral force capacity can be calculated as:

$$F=\lambda\cdot W \quad (14)$$

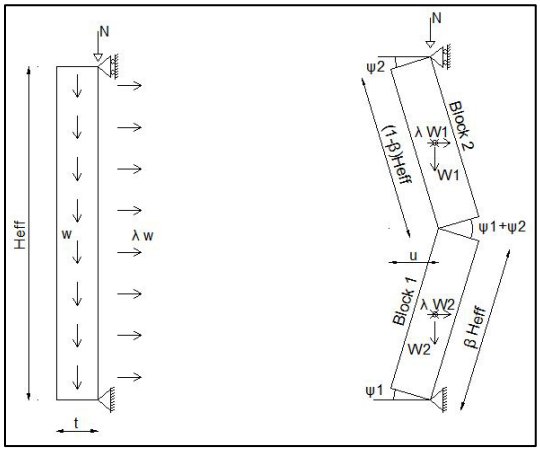

Figure 34 – Rigid blocks model for simply supported wall.

Following Derakhshan [8], the lateral pressure at onset of cracking (first crack lateral pressure) w_{cr} can be estimated as:

$$w_{cr} = \frac{f_{x1} + \sigma_v + 0.5\frac{W}{L_w t_w} + \sqrt{(f_{x1} + \sigma_v)\cdot\left(f_{x1} + \sigma_v + \frac{W}{L_w t_w}\right)}}{1.5\left(\frac{H_{eff}}{t_w}\right)^2} \quad (15)$$

where f_{x1} is the masonry flexural strength with the moment vector parallel to the bed joints and in the plane of the wall and σ_v is the overburden.
The lateral force at onset of cracking F_{cr} can be calculated as:

$$F_{cr} = w_{cr} \cdot L \cdot H_{eff} \quad (16)$$

8.2 Estimation for two-way bending mechanism

Several approaches are available in literature for the estimation of the capacity of a wall subject to two-way bending failure mechanism. In this Section, the methods proposed by the Australian Standard (AS) [6] and the Eurocode 6 (EC6) [7] are considered.

8.2.1 Australian Standard method

The lateral load capacity of the wall can be estimated as suggested by the Australian standard AS3700 (equation 7.4.4.2 in [6]) as:

$$w_{AS} = \frac{2a_f}{L_d^2}\left(k_1 M_{ch} + k_2 M_{cd}\right) \tag{17}$$

where L_d is the design length that in case of both vertical edges laterally supported is equal to half of the actual length of the wall, a_f is the aspect factor (Table 14) and k_1 and k_2 are coefficients (Table 14). M_{ch} and M_{cd} are the horizontal bending moment capacity and the diagonal bending moment capacity per unit of length of diagonal crack, respectively, defined in Clause 7.4.3.2 and 7.4.4.3 [6]. For clay brick masonry, the horizontal bending moment capacity M_{ch} is calculated as the minimum of:

$$M_{ch} = \min\begin{cases} 2.0 \cdot \Phi \cdot k_p \cdot \left(\sqrt{f_{mt}^{'}}\right) \cdot \left(1 + \frac{f_d}{f_{mt}^{'}}\right) \cdot Z_d \\ 4.0 \cdot \Phi \cdot k_p \cdot \left(\sqrt{f_{mt}^{'}}\right) \cdot Z_d \\ \Phi \cdot \left(0.44 \cdot f_{ut}^{'} \cdot Z_u + 0.56 \cdot f_{ut}^{'} \cdot Z_p\right) \end{cases} \tag{18}$$

For calcium silicate element masonry, the formulation proposed in the standard for masonry with thin-layer mortar joints is considered:

$$M_{ch} = \Phi \cdot \left(0.22 \cdot f_{ut}^{'} + 0.33 \cdot f_{ut}^{'}\right) Z_d \tag{19}$$

where Φ is the capacity reduction factor (Clause 4.4 in [6]), k_p is a perpend spacing factor (Clause 7.4.3.4 in [6]), f'_{mt} is the characteristic flexural tensile strength (Clause 3.3.3 in [6]), f_d is the minimum design compressive stress on the bed joints (Clause 7.4.3.3 in [6]), f'_{ut} is the characteristic lateral modulus of rupture of the masonry units (Clause 3.2 in [6]), Z_d is the section modulus of the bedded area, Z_u is the lateral section modulus of masonry units and Z_p is the lateral section modulus based on the mortar contact area of the perpend joints (Clause 7.4.3.2 in [6]).

The diagonal bending moment capacity per unit of length of diagonal crack M_{cd} is calculated as:

$$M_{cd} = \Phi \cdot f_t^{'} \cdot Z_t \tag{20}$$

where f'_t is the equivalent characteristic torsional strength and Z_t is the equivalent torsional section modulus measured normal to the diagonal crack line (Clause 7.4.4.3 in [6]).

Table 14 – Coefficients for out-of-plane lateral load resistance (part of Table 7.5 in Ref. [6]).

Opening	No. vertical edges supported	Slope factor α	Aspect factor a_f	k_1	k_2
No	Both	≤1	$\frac{1}{\left(1-\frac{\alpha}{3}\right)}$	$\frac{R_{f1}+R_{f2}}{2}+1-\alpha$	$\alpha\left(1+\frac{1}{G_c^2}\right)$
No	Both	>1	$\frac{\alpha}{\left(1-\frac{1}{3\alpha}\right)}$	$\frac{R_{f1}+R_{f2}}{2}$	$1+\frac{1}{G_c^2}$

The coefficients a_f, k_1 and k_2 depend on the slope factor α, which identifies the slope of the diagonal cracks with respect to the horizontal bed joints. It should be noted that the slope factor α plays an important role in the estimation of the maximum lateral force. The slope factor α is calculated as required by Clause 7.4.4.2 in Ref. [6] as:

$$\alpha = \frac{G_c L_d}{H_d} \tag{21}$$

where design height H_d is half of the height of the wall, if the top edge is not free, and G_c is the assumed slope of the crack line for half-overlap stretcher bonding equal to:

$$G_c = \frac{2\left(h_u + t_j\right)}{l_u + t_j} \tag{22}$$

where h_u and l_u are the height and the length of the masonry unit, respectively, and t_j is the thickness of the mortar joint.
The coefficient k_1 depends also on the restraint factors R_{f1} and $R_{f2.}$ for the first and second supported edges of the wall. The values of R_{f1} and $R_{f2.}$ are equal to zero if there is no rotational restraint (hinged edges).
The lateral force capacity calculated following the Australian standard results:

$$F_{AS} = w_{AS} \cdot H_w \cdot L_w \tag{23}$$

where w_{AS} is the lateral load capacity of the wall and H_w and L_w are the height and length of the wall, respectively.

8.2.2 Eurocode 6 method

The moment of a masonry wall loaded in two-way bending when the plane of failure is parallel to the bed joints in the f_{x1} direction is calculated using Eq. 5.17 in Eurocode 6[7]:

$$M_{E,1} = \alpha_1 w_E L_w^2 \tag{24}$$

where w_E is the lateral load per unit area, α_1 is the bending moment coefficient taking into account the degree of fixity at the edges of the walls and the height to length ratio of the walls and L_w is the length of the wall.

The moment of a masonry wall loaded in two-way bending when the plane of failure is perpendicular to the bed joints in the f_{x2} direction is calculated according to equation 5.18 of [7]. The equation is reported below:

$$M_{E,2} = \alpha_2 w_E L_w^2 \tag{25}$$

where α_2 is the bending moment coefficient the taking into account the degree of fixity at the edges of the walls, the height to length ratio of the walls.

In Eurocode 6 it is stated that the coefficients α_1 and α_2 for single leaf walls with a thickness less or equal to 250 mm may be obtained from Annex E as $\alpha_1=\eta\,\alpha_2$, where $\eta=f_{x1}/f_{x2}$ is the orthogonal ratio of the flexural strengths of the masonry. Annex E gives for different boundary conditions the value of α_2, based on the ratio H_w/L_w and η. The support conditions used in the tests (clamped at top and bottom and hinged at the sides) are not given, so the horizontal force for walls support conditions defined as E (hinged on all sides) and I (clamped on all sides) will be calculated. These values should be considered as upper and lower bounds of the experimental results.
The lateral load per unit area w_E is:

$$w_{E,1} = \frac{f_{x,1} Z}{\alpha_1 \cdot L_w^2} \tag{26}$$

$$w_{E,2} = \frac{f_{x,2} Z}{\alpha_2 \cdot L_w^2} \tag{27}$$

where Z is the elastic section modulus of unit height or length of the wall. $w_{E,1}$ and $w_{E,2}$ give the same results because $\alpha_1=\eta\,\alpha_2$ and $\eta=f_{x1}/f_{x2}$.
The lateral force capacity calculated in agreement with Eurocode 6 results:

$$F_{EC6} = w_E \cdot H_w \cdot L_w \tag{28}$$

where w_E is the lateral load per unit area and H_w and L_w are the height and length of the wall.

8.3 Comparison with experimental results

In this section the experimental results are compared in terms of lateral force with the analytical results, derived in Section 0 and 8.2 for the one-way and the two-way bending failure mechanism, respectively.

8.3.1 One way bending

The lateral force at onset of cracking F_{cr} and maximum lateral force capacity F for specimen TUD_COMP-28 are evaluated using Eqs. (16) and(14), respectively. The input parameters used in the calculation are reported in Table 15. The analytical and experimental results are compared in Table 16 and Figure 35.

The experimental lateral force at onset of cracking of 10.0 kN matches well with the estimation value of 9.2 kN. For the comparison, the experimental capacity has been determined when a crack opening higher than 0.01 mm has been observed for the first time (Section 6.2.1).

By adopting the rigid block model, the maximum lateral force results equal to 17.7 kN. This value results lower than the one measured experimentally (+20.7 kN and –18.0 kN). As discussed in Section 5.3, the mismatch between experimental and analytical results can be caused by the presence of inflated airbags on the tension side of the wall. To confirm this aspect additional investigation are required. However, it can be noticed that in the post-peak phase the degradation of the capacity experimentally recorded follows the same trend of the rigid block model. Additionally, by considering the capacity of the wall for negative displacements an agreement between experimental and analytical results is observed.

Table 15 - Parameters for the analytical calculation for TUD_COMP-28

Parameter	Symbol	Unit	Value
Wall length	L_w	mm	1448
Wall thickness	t_w	mm	120
Wall effective height	H_{eff}	mm	2585
Coefficient	β	-	0.5
Overburden	σ_V	MPa	0.25
Pre-compression force	N	kN	43.4
Self-weight of the wall	W	kN	8.6
Masonry flexural strength with the moment vector parallel to the bed joints and in the plane of the wall	f_{x1}	MPa	0.58
Self-weight multiplier	λ	-	2.05

Table 16 - Estimation of the maximum capacity and cracking capacity for wall TUD_COMP-28.

Parameter		Units	Analytical	Experimental
Lateral force at onset of cracking	$F_{cr} = w_{cr} L H_{eff}$	kN	9.2	10.0
Lateral force capacity	$F = \lambda W$	kN	**17.7**	**-18.0**

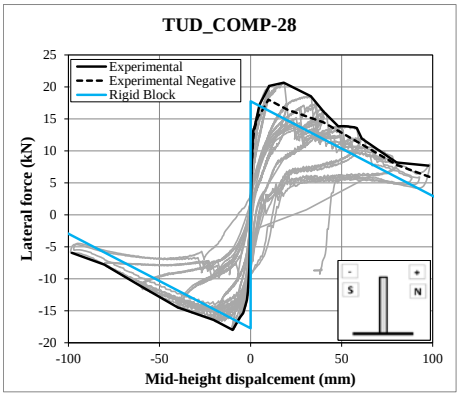

Figure 35 – Capacity curve for wall TUD_COMP-28: experimental envelope curve and rigid block model.

8.3.2 Two way bending

The lateral force capacity of the specimens TUD_COMP-26, TUD_COMP-27 and TUD_COMP-29 is evaluated according to Section 8.2. The input parameters necessary for the application of the two methods, the analytical estimations and the comparison with the experimental results are shown in Table 17 and Table 18. It should be pointed out that the formulation proposed by both the Eurocode 6 and the Australian Standard are formulated for single wythe walls. Currently, no standardised formulation for multi wythe walls is available in these standards. Moreover, the Australian standard considers only walls with an half-overlap bond pattern.

Table 17 – Comparison of the experimental lateral force capacity and the Eurocode 6 prediction for the two-way bending walls.

Eurocode 6				
Specimen name	-	TUD_COMP-26	TUD_COMP-27	TUD_COMP-29
η	-	0.25	0.34	0.79
H_w/L_w	-	0.69	0.71	0.76
α_2 hinged all sides (Annex E table E)	-	0.055	0.049	0.035
α_2 clamped all sides (Annex E table I)	-	0.028	0.024	0.017
w_E Hinged	kPa	1.27	4.17	3.83
w_E Clamped	kPa	2.51	8.37	7.81
F_{EC6} Hinged	kN	**13.6**	**43.4**	**37.6**
F_{EC6} Clamped	kN	**26.8**	**87.1**	**76.6**
Experimental				
$F_{cr,-}$	kN	**-20.0**	**-78.3**	**-**
Percentage error				
Percentage error – Hinged	%	**-32%**	**-45%**	**-**
Percentage error – Clamped	%	**34%**	**11%**	**-**

Table 18 – Comparison of the experimental lateral force capacity and the Australian standard prediction for the two-way bending walls.

Australian Standard				
Sample	-	TUD_COMP-26	TUD_COMP-27	TUD_COMP-29
α	-	0.795	0.773	1.894
G_c	-	0.55	0.55	1.43
$\varphi=atan(G_c)$	Deg	29	29	55
a_f	-	1.36	1.35	2.30
k_1	-	0.205	0.227	0
k_2	-	3.467	3.371	1.486
M_{cd} (KNm/m)	kNm/m	0.51	1.15	3.25
M_{ch} (KNm/m)	kNm/m	2.02	4.37	2.39
w_{AS}	kPa	1.53	3.56	6.87
F_{AS}	kN	**16.3**	**37.0**	**67.3**
Experimental				
F_{max} -	kN	**-36.1**	**-78.3**	**-**
Error				
Error (negative)	%	**-55%**	**-53%**	**-**

The formulation proposed by Eurocode 6 provides an estimation of the elastic bending moment. Consequently, the obtained lateral force capacity F_{EC6} is comparable with the experimental lateral force at onset of cracking F_{cr}, evaluated considering the first visible decreasing in stiffness. By adopting the formulation proposed in Eurocode 6 for the boundary conditions as hinged at all sides and as clamped at all sides, lower and upper bounds can be defined. Although the formulation is simple its application requires knowledge on the flexural strengths of masonry (f_{x1} and f_{x2}).

The Australian standard, based on the virtual work method, provides the maximum lateral force capacity starting from the evaluation of the bending moments capacities due to cracks formation. The crack pattern is determined by the value of the slope factor α (Eq. (21)); if the slope factor α is less than one the failure crack pattern will have a central vertical crack, otherwise a central horizontal crack will occur. If a crack pattern with central vertical crack is predicted (α<1), the lateral capacity is defined as the contribution of both the diagonal, M_{cd}, and the horizontal, M_{ch}, bending moment capacities (Figure 36a). On the contrary if a crack pattern with central horizontal crack is predicted (α≥1), the lateral capacity is defined as the contribution of only the diagonal bending moment capacity M_{cd} and no contribution of the vertical bending moment M_{cv} is considered (Figure 36b).

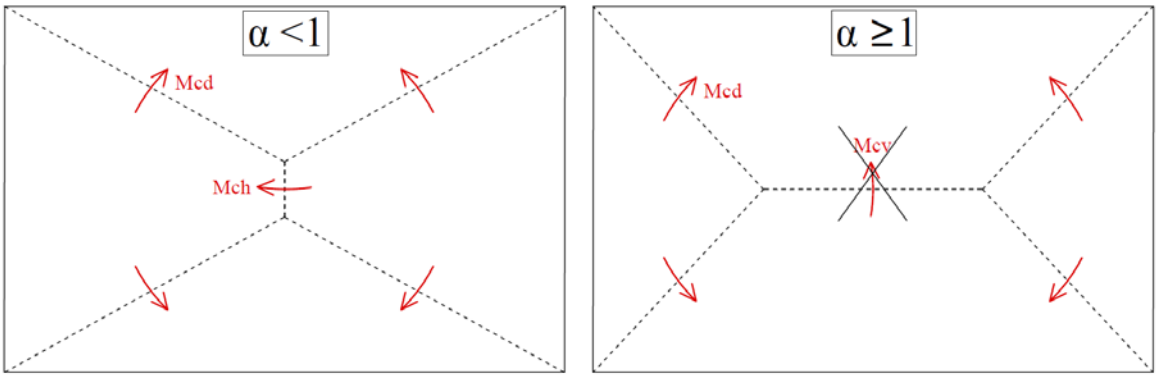

(a) (b)

Figure 36 – Australian standard: (a) slope factor α<1 and (b) slope factor α≥1

The formulation proposed by the Australian standard (AS) provides an underestimation of approximatively 55% of the lateral force capacity for both single wythe (TUD_COMP-26) and double wythe (TUD_COMP-26) clay brick masonry walls. In both cases, the predicted crack pattern consist of a vertical central crack, which is not in agreement with the experimental findings (Figure 37). It should be noted that the capacity reduction factor Φ for the design has not been considered.

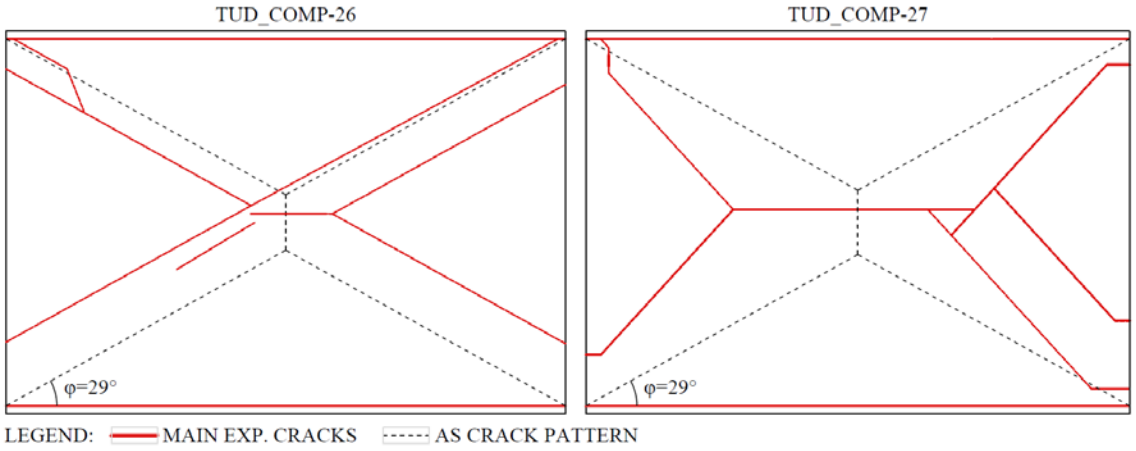

(a) (b)

Figure 37 – Experimental, theoretical according to AS and theoretical according to modified AS crack pattern of: (a) TUD_COMP-26 and (b) TUD_COMP-27

9 Assessment procedure proposed by NPR 9998:2017

In this Section, the assessment procedure for out-of-plane mechanism proposed in the NEN-NPR 9998:2017 [9] is analysed and comparison with respect to the experimental findings.

The out-of-plane assessment of masonry walls using the non-linear kinematic analysis (NLKA) is proposed in Annex H of NEN-NPR 9998:2017. The method is based on the principle of virtual work and the failure mechanism of masonry walls spanning one-way vertically is considered. Considering an unreinforced masonry wall subjected to a uniform inertial face loading, the seismic coefficient for the wall where the capacity equals the seismic demands ξ_{SCC} has to be higher than the design seismic coefficient for the wall $S_{a;d}$. The capacity of the wall at near collapse should be estimated at a displacement equal to the 60% of the instability displacement. In order to evaluate, the coefficient ξ_{SCC} at near collapse, the standard provides curves as a function of the geometry and the overburden to self-weight ratio of the wall.

Considering the tested wall, the range of the provided curves is insufficient, consequently the formulation in Annex H cannot be applied. The nonlinear kinematic analysis is thus performed by considering the prescription in Annex G, but still following the same assumption prescribed in Annex H.
For each wall, the capacity has been determined by considering the rigid-block model, presented in Section 8.1, that follows the same assumptions made in Annex H [9]. The near collapse limit state is defined at 60% of the instability displacement, which is $t_w/2$ [10]. For comparison the capacity of the wall derived experimentally has been also reported by considering that the effective modal mass was 100% of the self-weight of the wall.
The seismic demand has been defined by considering the wall as part of a building located in Loppersum (Table 19), one of the city in the Netherlands with higher seismic demand. The elastic demand acceleration displacement response spectrum curve (ADRS) has been determined combining the elastic acceleration response spectrum (see G.7.2 of [9]) and the elastic displacement response spectrum (see 3.2.2.2.1 of [9]). In Annex H, the seismic demand is increased in order to consider for the position of the wall in the building and the relative dynamic response between the wall and the building. Similarly, the elastic demand acceleration displacement response spectrum curve has been amplified. The following amplification factor $S_{a;d}/\alpha$ has been considered:

$$S_{a;d}/\alpha = \left[\frac{3 \cdot \left(1 + \frac{z}{H_{building}} \right)}{1 + \left(1 - \frac{T_a}{T_1} \right)^2} - 0.5 \right] \geq 1.0 \qquad (29)$$

where z is the height of gravity centre of the wall above top of the foundation, $H_{building}$ is the height of the building above top of the foundation, T_1 is the fundamental period of the building and T_a is the fundamental period of the wall.

Table 19– Loppersum spectrum data according to NEN-NPR 9998-webtool.

Parameters	Symbol	Units	Value
Peak soil acceleration at ground level considering soil factor	$\mathbf{a_gS}$	g	0.3203
Relationship between peak ground acceleration and the plateau value of the elastic response spectrum	**p**	-	1.67
Lower limit of the period of the constant spectral acceleration branch	$\mathbf{T_B}$	s	0.255
Upper limit of the period of the constant spectral acceleration branch	$\mathbf{T_C}$	s	0.618
Value defining the beginning of the constant displacement response range of the spectrum	$\mathbf{T_D}$	s	1.077

Figure 38 summarizes the adopted method. If the near collapse displacement capacity u_{NC} is higher than the displacement demand u_{demand} the wall can withstand the seismic demand. By imposing that the displacement capacity equals the displacement demand ($u_{NC}=u_{demand}$), the critical amplification ($S_{a;d}/\alpha$)$_{cr}$ factor is calculated.

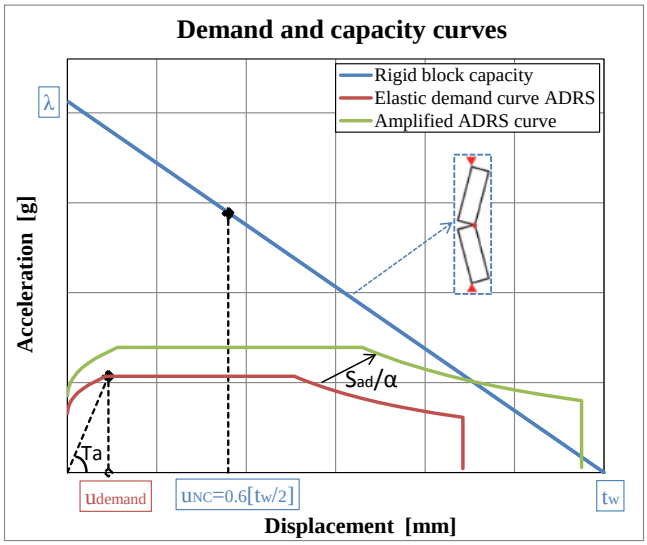

Figure 38 – Explicative scheme of for the NLKA.

Figure 39 shows the elastic demand curve (ADRS) and the capacity curves for each wall. By considering the assumption of one-way vertically spanning wall, for all cases the capacity results higher than the demand ($u_{NC}>u_{demand}$). By considering the capacity of the wall as determined experimentally, it is possible to note that the actual capacity of the walls subject to two-way bending mechanisms is approximately 4 times higher than the maximum acceleration given by the ASRS curve. This difference between capacity and demand is higher than the one obtained with the assumption of the one-way vertically spanning wall.

In order to evaluate the impact of the assumption of the one-way vertically spanning wall, the critical amplification factor has been calculated considering both this assumption as well as the experimentally determined capacity of the wall.
Figure 40 shows the critical amplification calculated assuming the one-way vertically spanning wall. The critical amplification factor $(S_{a;d}/\alpha)_{cr,rigid\_block}$ at which the demand equals the capacity is equal to 1.1, 2.3, 3.9 and 1.2 for specimen TUD_COMP-26, TUD_COMP-27, TUD_COMP-28 and TUD_COMP-29, respectively. From this figure it is possible to note that if the period of the wall T_a is between T_B and T_C, the nonlinear kinematic analysis returns the same response of a simpler linear kinematic analysis. By comparing the two analysis methods for the selected case, it is obvious that the period of the wall is defined such that this correspondence is met.
By comparing the experimental capacity of the wall and the acceleration given by the ASRS curve in the philosophy of a linear kinematic analysis, the critical amplification factor results equal to 3.8, 4.1 and 3.9 for specimen TUD_COMP-26, TUD_COMP-27, TUD_COMP-28, respectively.

To show the influence of the critical amplification factor, the following case studies are considered: a one-story high building in which the wall is located at ground floor ($z/H_{building}=0.26$) and a two-story high building in which the wall is located at first floor ($z/H_{building}=0.54$). Considering the critical amplification factor determined with the assumption of a one-way vertically spanning wall and the experimental capacity, the maximum building period T_1 for which the wall can withstand the seismic demand can be calculated (Figure 41). Considering the assumption of one-way vertically spanning wall, the considered walls can withstand the amplified demand if they are located in buildings with a period lower than approximatively 0.2 s in both case studies. However, if the experimental for wall showing two-way bending mechanisms is considered, the walls can withstand the amplified demand if they are located in one-story high buildings with a period lower than approximatively 0.5 s or if they are located in two-story high buildings with a period lower than approximatively 0.4 s (Figure 41a,b). These limits are approximatively 1.5 times higher with respect to the limits considering the one-way vertically spanning wall.

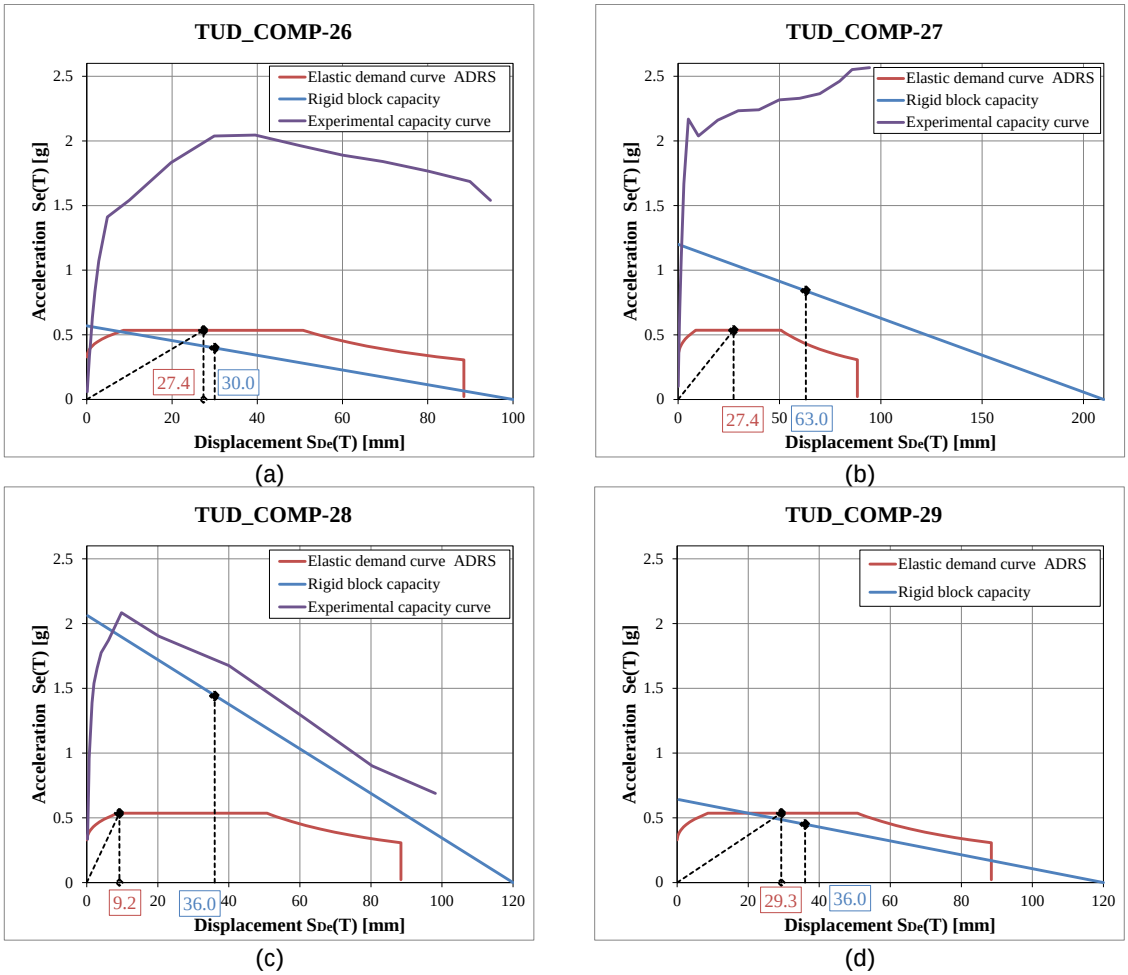

Figure 39 – Application NEN-NPR 9998:2017 for the case of Loppersum: (a) two-way bending single wythe clay masonry wall (TUD_COMP-26), (b) two-way bending double wythe clay masonry wall (TUD_COMP-27), (c) one-way bending calcium silicate element wall (TUD_COMP-28) and (d) two-way bending calcium silicate element wall (TUD_COMP-29).

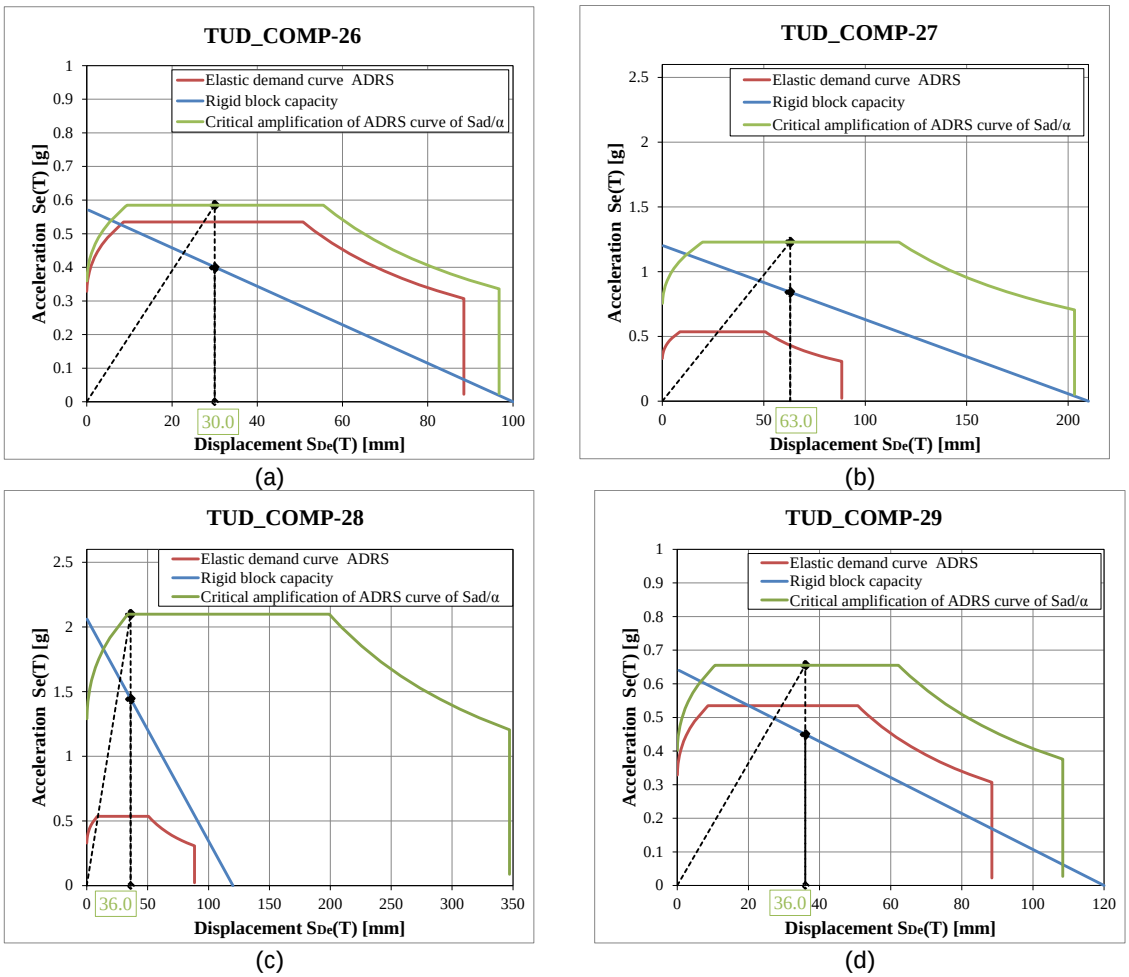

Figure 40 – Critical amplification factor for: (a) two-way bending single wythe clay masonry wall (TUD_COMP-26), (b) two-way bending double wythe clay masonry wall (TUD_COMP-27), (c) one-way bending calcium silicate element wall (TUD_COMP-28) and (d) two-way bending calcium silicate element wall (TUD_COMP-29).

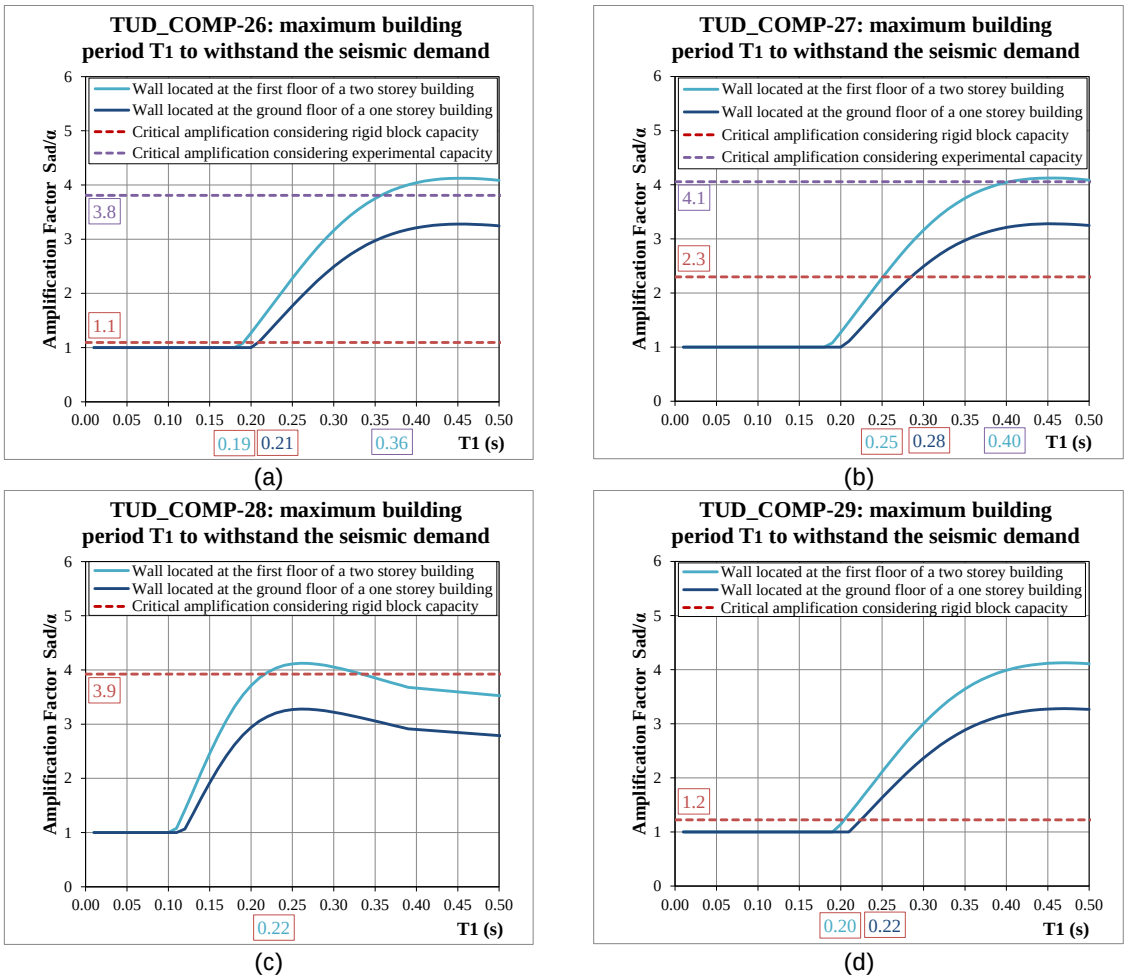

Figure 41 – Maximum building period to withstand the seismic demand: (a) two-way bending single wythe clay masonry wall (TUD_COMP-26), (b) two-way bending double wythe clay masonry wall (TUD_COMP-27), (c) one-way bending calcium silicate element wall (TUD_COMP-28) and (d) two-way bending calcium silicate element wall (TUD_COMP-29).

10 Summary and conclusions

Four quasi-static out-of-plane bending tests have been carried out at Stevin II laboratory of Delft University of Technology within the NAM Structural Upgrading project 2016/2017. Table 20, Figure 42, Figure 43 and Figure 44 show an overview of the results in terms of envelope curves, maximum lateral force, initial stiffness and crack pattern. Due to technical problems, for wall TUD_COMP-29 only information on its initial stiffness were determined.

Table 20 – Overview of the properties and results of the performed out-of-plane tests.

Sample name	Masonry type and dimension	Boundary conditions	Overburden	Initial stiffness	Lateral Force	
					F^+	F^-
	mm		MPa	kN/mm	kN	kN
TUD_COMP-26	Solid clay brick masonry 3950x2710x100	2-way OOP	0.06	9.6	+37.1*	-36.1
TUD_COMP-27	Solid clay brick masonry 3840x2710x210	2-way OOP	0.06	41.4	+89.5*	-78.3
TUD_COMP-28	CS elements 1448x2725x120	1-way OOP	0.25	12.3	+20.7	-18.0
TUD_COMP-29	CS elements 3597x2725x120	2-way OOP	0.06	15.9	-	-

* Corrected value in order to take the lateral force increment due to the friction between airbags and wall on the tension side of the wall (Section 5.3)

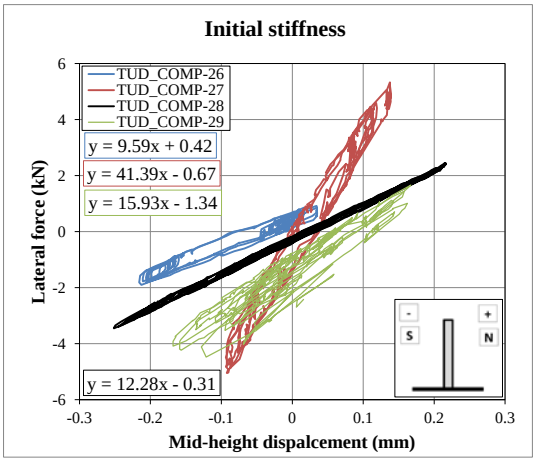

Figure 42 – Initial stiffness of specimens TUD_COMP-26 ,TUD_COMP-27, TUD_COMP-28 and TUD_COMP-29.

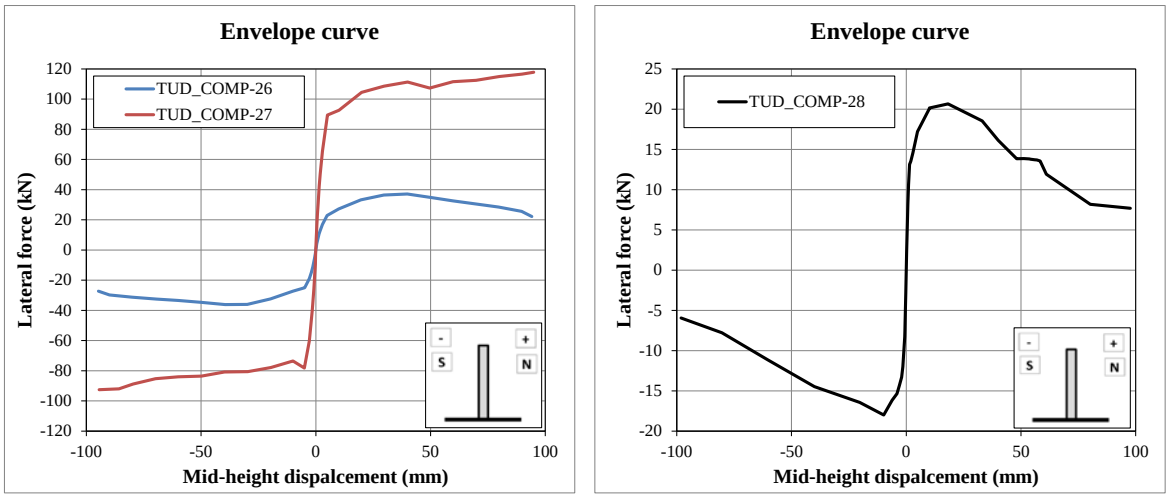

(a) (b)

Figure 43 – Envelope curve of wall subject to: (a) two-way bending tests (TUD_COMP-26,-27); (b) one-way bending test (TUD_COMP-28).

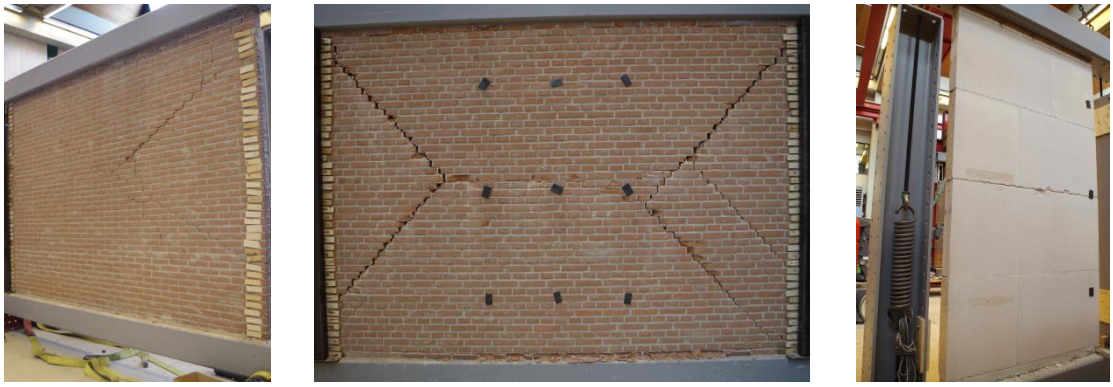

(a) (b) (c)

Figure 44 – Crack pattern for specimens: (a) TUD-COMP_26; (b) TUD-COMP_27; (c) TUD-COMP_28.

By observing the experimental results, the following conclusions can be drawn:

- In the adopted loading procedure, the airbags on the South and North sides are pumped up to a certain initial pressure before stating the test. During the test the initial pressure is kept constant in the airbags on the North side, while the pressure increases in the airbags on the South side due to imposed displacement. The constant pressure, kept on the tension side of the deformed wall, provokes an increment in lateral force due to friction mechanism. As a results, the capacity curve presents an asymmetric behaviour in forces, showing higher values in the positive loading direction. Consequently, the capacity curve for negative displacement better represents the real behaviour of the wall.
- By analysing the displacement profile and the initial stiffness of the wall, considerations on the applied boundary conditions can be made. It can be concluded that in the one-way bending the top boundary condition can be approximated as an hinged connection while bottom boundary condition can be considered as a clamped condition. In the case of the two-way bending, both top and bottom boundary conditions can be approximated as hinges.
- By comparing the one-way bending test (TUD_COMP-28) with the two-way bending tests (TUD_COMP-26 and TUD_COMP-27) it can be observed a different crack pattern and a different degradation in capacity. The crack pattern at the final stage of the one-way wall was characterized by three horizontal cracks located at the bottom, mid-height and top bed joint whilst the crack pattern of the two-way bending walls was characterized by the typical X-shaped, consisting of a central horizontal crack from which diagonal cracks branched to the corners of the wall. Differently

from the two-way bending tests, in the one-way bending test after the maximum lateral force was reached a fast degradation in force was observed in both loading directions.

- By comparing the two-way bending tests on the single wythe (TUD_COMP-26) and double wythe (TUD_COMP-27) clay brick masonry walls, it can be observed that the double wythe wall shows a lateral force capacity two times higher than the single wythe wall and an initial stiffness four times higher than the single wythe wall. After the maximum lateral force was reached, a slightly reduction in force was observed for the single wythe wall (TUD_COMP-26) and a slightly increase in force was observed for the double wythe wall (TUD_COMP-27). The crack pattern results similar for the two walls, with the difference that in the case of a double wythe wall the central horizontal crack is longer. It should be noted that, differently from the single wythe wall, the double wythe wall was tested only up to a displacement of 100 mm, corresponding approximatively to 50% of the wall thickness. The limited degradation in capacity in the post-peak phase for both walls it suggests that the lateral restraints work similarly to the real boundary condition characterized by return walls [9].

By comparing the experimental and analytical results in the case of the one-way bending failure mechanism the following conclusions can be drawn:

- The experimental lateral force at onset of cracking matches well with the estimation value obtained using the formulation proposed by Derakhshan [8].
- By adopting the rigid block model, the degradation of the capacity experimentally recorded follows the same trend of the rigid block model, but the calculated maximum lateral force is lower than the one measured experimentally. The mismatch between experimental and analytical results can be caused by the presence of inflated airbags on the tension side of the wall. To confirm this aspect additional investigation are required.

By comparing the experimental and analytical results in the case of the two-way bending failure mechanism the following conclusions can be drawn:

- The method proposed by the Australian standard provides a large underestimation (approximatively -55%) of the lateral force capacity. This is the result of the incorrect prediction of the crack pattern and of the excluding in the contribution of the vertical bending moment with respect to the horizontal crack. The method should be improved for further applications.
- The formulation proposed by Eurocode 6 can be applied only to estimate the lateral force at onset of cracking. The formulation provides upper and lower bounds for the estimation of the lateral capacity, because it considers the only the condition of 4 clamped sides and the condition of 4 hinged sides.
- It should be pointed out that the formulation proposed by the Australian Standard and the Eurocode 6 are both formulated for single wythe walls. Currently, no standardised formulation for multi wythe walls is available in these standards.

Eventually, the Dutch code NEN-NPR 9998:2017 has been applied by considering the tested walls as part of a building located in Loppersum. The following remarks can be made:

- For the tested wall was not possible to apply the prescriptions given by Annex H. However, a similar procedure in the spite of Annex G was performed.
- The standard does not provide a method to estimate the capacity of the two-way bending mechanism. By considering the approximation of one-way vertically spanning walls, the capacity of two-way spanning walls is largely underestimated.
- The only formulation currently available to estimate the lateral force capacity of two-way spanning walls is provided by the Australian standard. However, the current formulation largely underestimates the capacity of the tested walls in comparison with experimental findings. Additionally, if this formulation is compared with the analytical formulation for one-way vertically spanning walls, a significant improvement in the lateral capacity estimation is not obtained as shown in Figure 45 for wall TUD_COMP-26 and TUD_COMP-27.

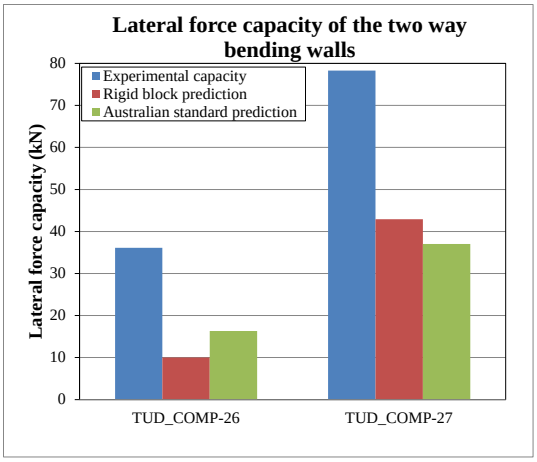

Figure 45 – Lateral force capacity of the two-way bending walls: experimental results (blue), analytical estimate considering one-way vertically spanning wall (red), analytical estimate considering two-way spanning wall following the Australian standard (green).

Following the drawn conclusions on the interpretation of the experimental findings and the evaluation of available analytical models for the prediction of the lateral capacity of walls subject to out-of-plane loading, the formulation of an efficient analytical models to capture the two-way bending mechanism is needed. In order to fulfil this aim, it is suggested to carried out additional quasi-static cyclic two-way out-of-plane bending tests paying attention to the following aspects:

- boundary conditions (different sides restrains, different pre-compression levels)
- geometry of the wall (e.g. variation in length)
- presence of openings
- different masonry types, in particular single and multi wythe walls.

11 Reference

[1] Jafari, S., Esposito, R. (2017). Material tests for the characterisation of replicated solid clay brick masonry. Delft University of Technology. Report number C31B67WP1-12, version 01, 12 August 2017.

[2] Jafari, S., Esposito, R. (2017). Material tests for the characterisation of replicated calcium silicate element masonry. Delft University of Technology. Report number C31B67WP1-11, version 01, 11 August 2017.

[3] Ravenshortst, G., Messali, F. (2016) Out-of-plane tests on replicated masonry walls. Report version 4 of 30-05-2016, Delft University of Technology.

[4] Griffith, M.C., Vaculik, J., Lam, N.T.K., Wilson J., (2007). Cyclic testing of unreinforced masonry walls in two-way bending. Earthquake engineering and structural dynamics. 2007, 36:801-821.

[5] ASTM E2126-11 (2011). Standard Test Methods for Cyclic (Reversed) Load Test for Shear Resistance of Vertical Elements of the Lateral Force Resisting Systems for Buildings. ASTM International.

[6] AS 3700 (2011). Australian Standard – Masonry Structures.

[7] EN 1996-1-1+A1 (2013). Eurocode 6 – Design of masonry structures – Part 1-1: General rules for reinforced and unreinforced masonry structures.

[8] Derakhshan, H., Griffith, M.C., Ingham, J.M. (2013). Airbag testing of multi-leaf unreinforced masonry walls subjected to one way bending.

[9] NEN-NPR 9998 (2017). Assessment of structural safety of buildings in case of erection, reconstruction and disapproval - Basic rules for seismic actions: induced earthquakes. Nederlands Normalisatie-instituut.

[10] New Zealand Society for Earthquake Engineering (2016). The seismic assessment of existing buildings, Part C8: Seismic assessment of unreinforced masonry buildings. Wellington, New Zealand: MBIE, EQC, SESOC, NZSEE and NZGS.

[11] Griffith, M.C., Vaculik, J., Out-of-Plane Flexural Strength of Unreinforced Clay Brick Masonry Walls, TSM Journal, 2007, 25(1): 53-68.

Appendix A. Construction information

In this Section information on the construction of the walls are provided.

In this experimental campaign two masonry types are used: CS element masonry and solid clay brick masonry. Premixed mortar mixes are used in the construction. During the preparation of the mortar the following amount of water are used per bag of dry mix (25 kg): 6L for CS element masonry and 3.7L for solid clay brick masonry. A small concrete mixer is adopted for the preparation of the mortar. For each batch 6 and 1 bags of dry mix mortar are mixed for the, clay and CS element masonry respectively.

The wall is supported in a steel frame composed by a bottom and top beam. The first and last courses of masonry are glued on the beams with Sikadur-30 epoxy. In the case of the CS element masonry, a first kicker layer is adopted composed by small masonry units (Figure 46).

The drawings of each wall are reported in this appendix.

(a) (b)

Figure 46 – (a) Gluing of first course of masonry; (b) Small units used for the kicker layer in CS element masonry walls.

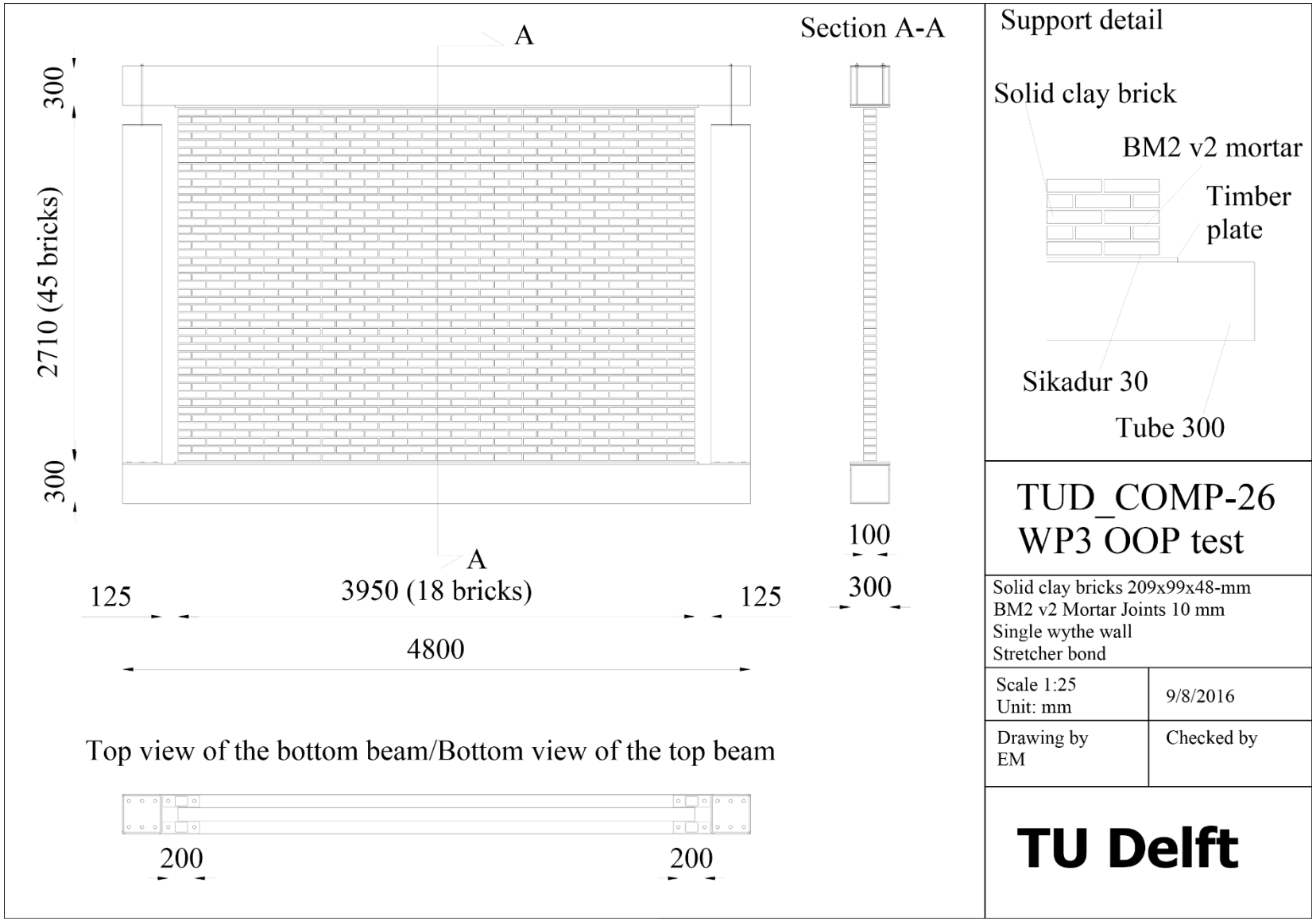
A
Section A-A
300
2710 (45 bricks)
300
A
100
300
125
3950 (18 bricks)
125
4800
Top view of the bottom beam/Bottom view of the top beam
200
200
Support detail
Solid clay brick
BM2 v2 mortar
Timber plate
Sikadur 30
Tube 300
TUD_COMP-26
WP3 OOP test
Solid clay bricks 209x99x48-mm
BM2 v2 Mortar Joints 10 mm
Single wythe wall
Stretcher bond
Scale 1:25
Unit: mm
9/8/2016
Drawing by
EM
Checked by
TU Delft

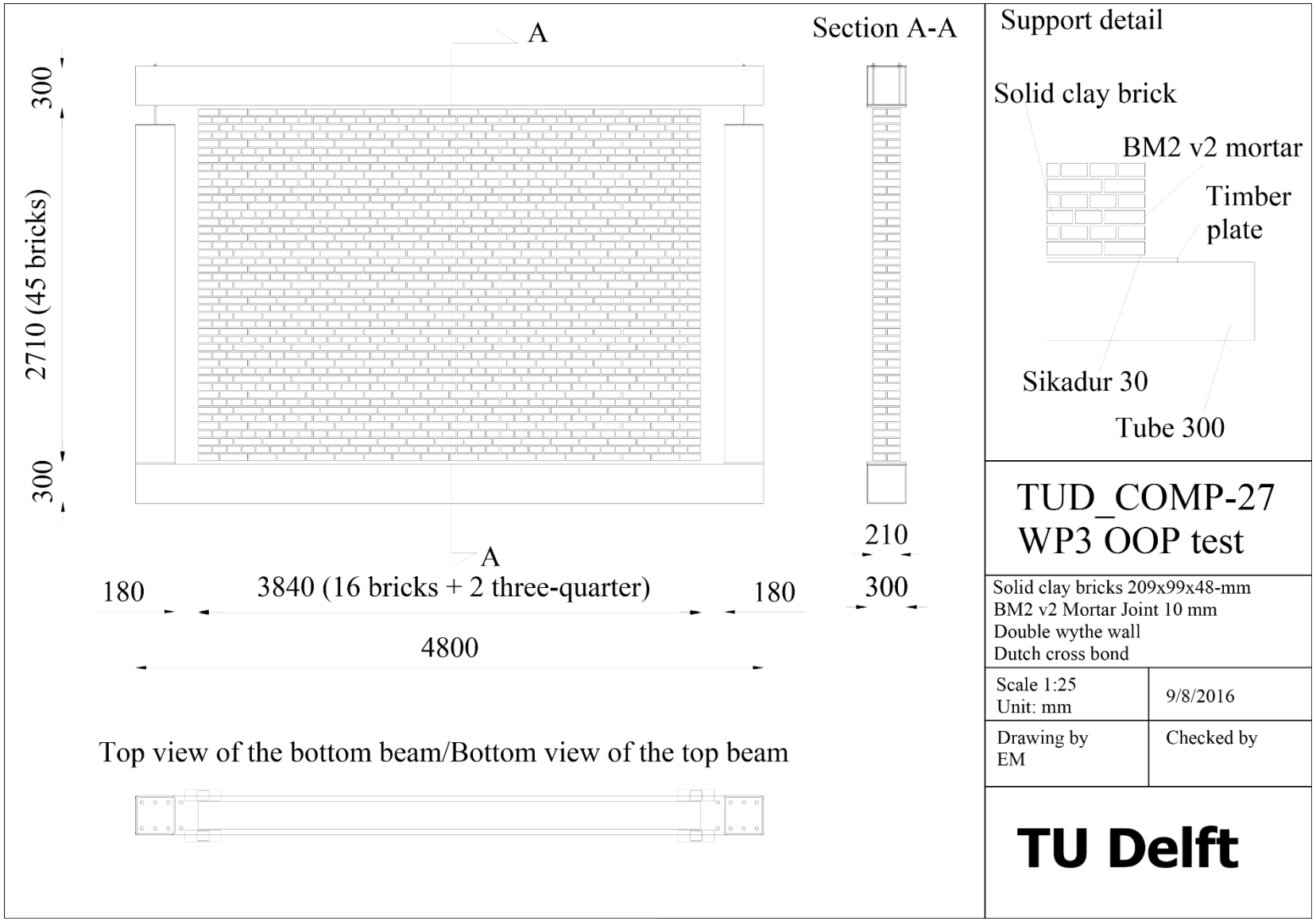
A
Section A-A
300
2710 (45 bricks)
300
210
A
180
3840 (16 bricks + 2 three-quarter)
180
300
4800
Top view of the bottom beam/Bottom view of the top beam
Support detail
Solid clay brick
BM2 v2 mortar
Timber plate
Sikadur 30
Tube 300
TUD_COMP-27
WP3 OOP test
Solid clay bricks 209x99x48-mm
BM2 v2 Mortar Joint 10 mm
Double wythe wall
Dutch cross bond
Scale 1:25
Unit: mm
9/8/2016
Drawing by
EM
Checked by
TU Delft

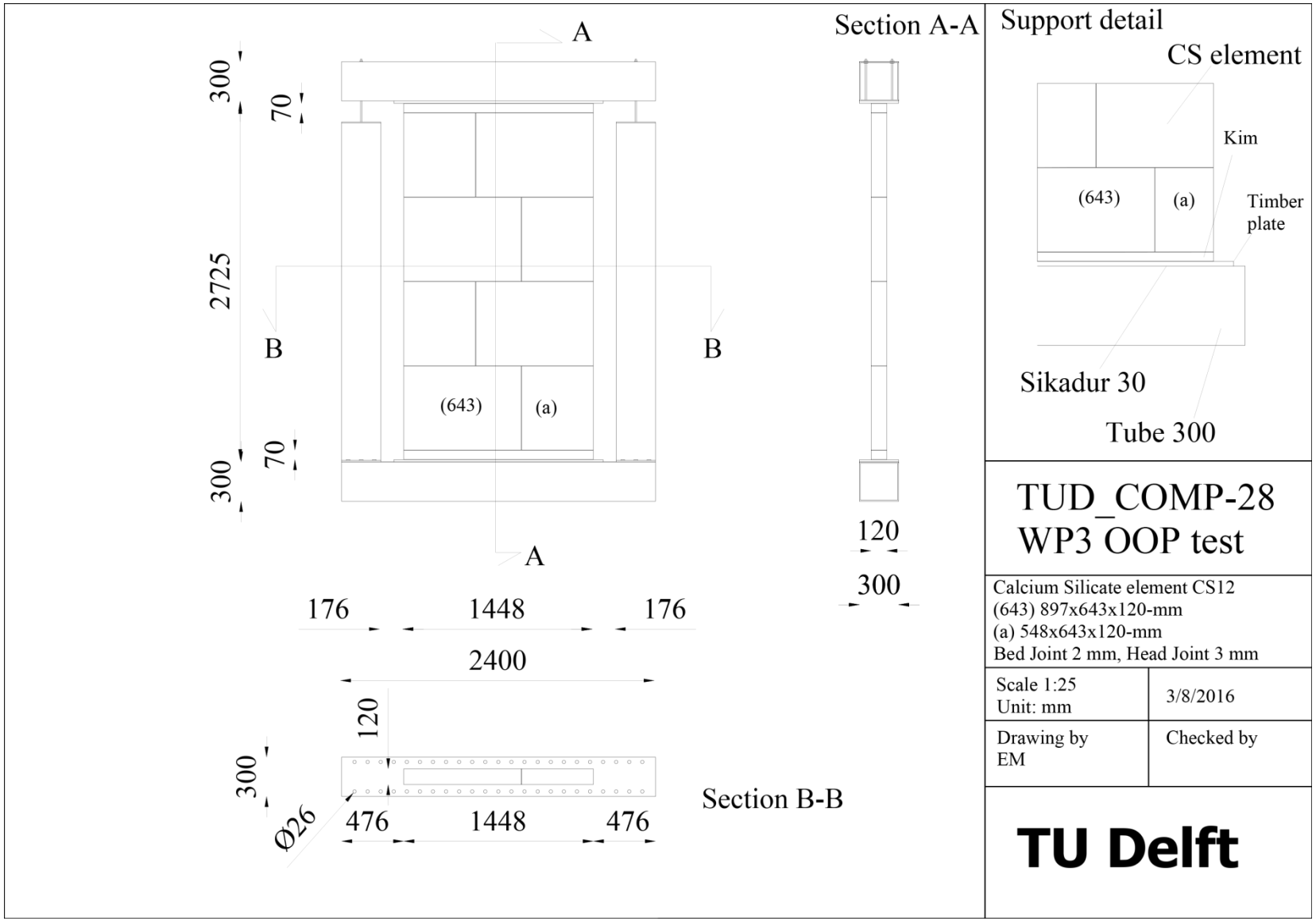
A
Section A-A
300
70
2725
B
B
(643)
(a)
300
70
A
120
300
176
1448
176
2400
120
300
Ø26
476
1448
476
Section B-B
Support detail
CS element
Kim
(643)
(a)
Timber plate
Sikadur 30
Tube 300
TUD_COMP-28
WP3 OOP test
Calcium Silicate element CS12
(643) 897x643x120-mm
(a) 548x643x120-mm
Bed Joint 2 mm, Head Joint 3 mm
Scale 1:25
Unit: mm
3/8/2016
Drawing by
EM
Checked by
TU Delft

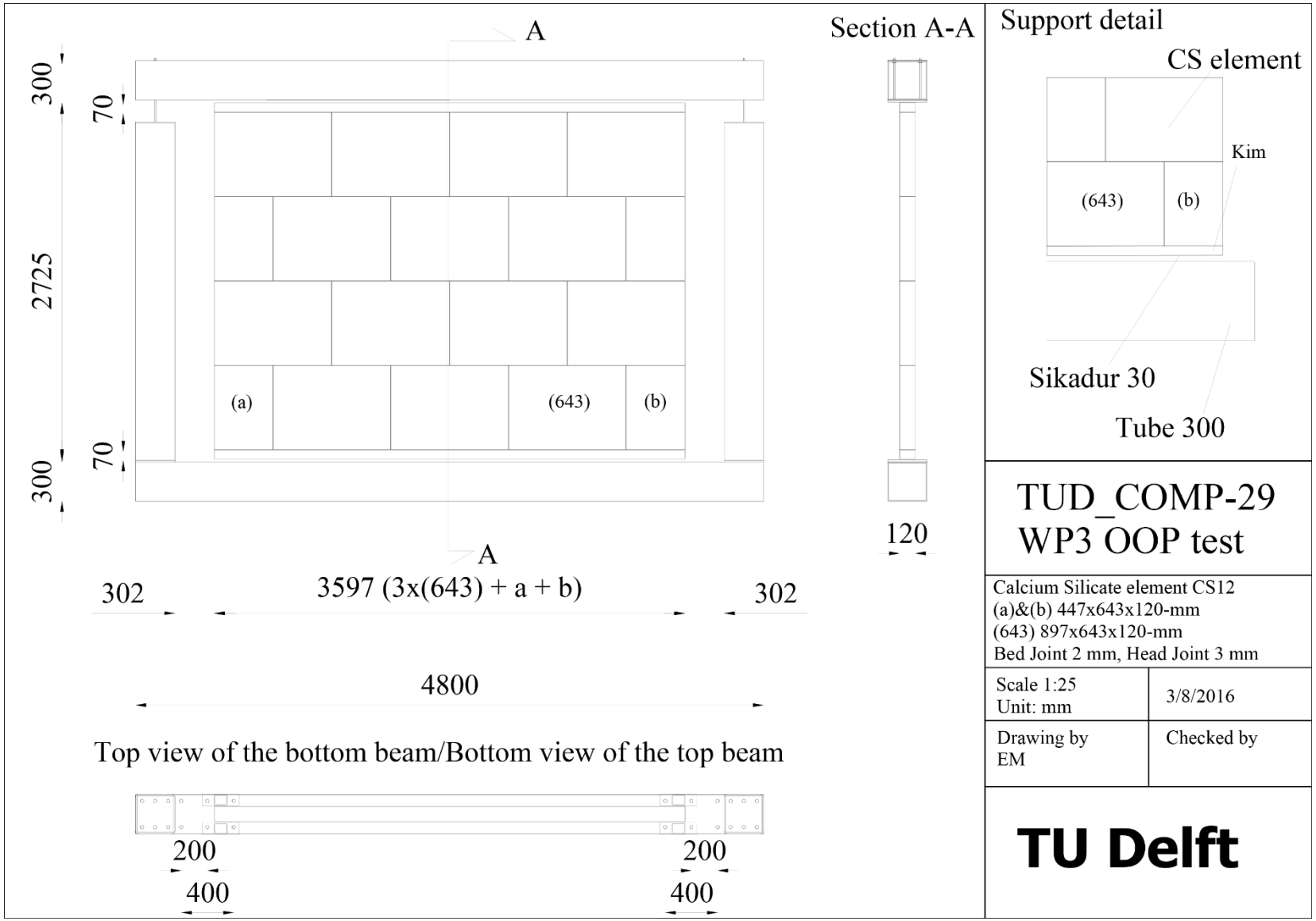
A
Section A-A
300
70
2725
300
70
(a)
(643)
(b)
120
A
302
3597 (3x(643) + a + b)
302
4800
Top view of the bottom beam/Bottom view of the top beam
200
200
400
400
Support detail
CS element
Kim
(643)
(b)
Sikadur 30
Tube 300
TUD_COMP-29
WP3 OOP test
Calcium Silicate element CS12
(a)&(b) 447x643x120-mm
(643) 897x643x120-mm
Bed Joint 2 mm, Head Joint 3 mm
Scale 1:25
Unit: mm
3/8/2016
Drawing by
EM
Checked by
TU Delft